



HAL
open science

**Sedimentological and Geochemical evidence for
Seismoturbidite Generation in the Kumburgaz Basin,
Sea of Marmara: Implications for Earthquake
Recurrence along the Central High Segment of the
North Anatolian Fault**

Nurettin Yakupoğlu, Gülsen Uçarkuş, K. Kadir Eriş, Pierre Henry, M. Namık
Çağatay

► **To cite this version:**

Nurettin Yakupoğlu, Gülsen Uçarkuş, K. Kadir Eriş, Pierre Henry, M. Namık Çağatay. Sedimentological and Geochemical evidence for Seismoturbidite Generation in the Kumburgaz Basin, Sea of Marmara: Implications for Earthquake Recurrence along the Central High Segment of the North Anatolian Fault. *Sedimentary Geology*, 2018, 380, pp.31-44. 10.1016/j.sedgeo.2018.11.002 . hal-01947384

HAL Id: hal-01947384

<https://hal.science/hal-01947384>

Submitted on 4 May 2019

HAL is a multi-disciplinary open access archive for the deposit and dissemination of scientific research documents, whether they are published or not. The documents may come from teaching and research institutions in France or abroad, or from public or private research centers.

L'archive ouverte pluridisciplinaire **HAL**, est destinée au dépôt et à la diffusion de documents scientifiques de niveau recherche, publiés ou non, émanant des établissements d'enseignement et de recherche français ou étrangers, des laboratoires publics ou privés.

1 **Sedimentological and Geochemical Evidence for Seismoturbidite Generation in the**
2 **Kumburgaz Basin, Sea of Marmara: Implications for Earthquake Recurrence along the**
3 **Central High Segment of the North Anatolian Fault**

4 Nurettin Yakupoğlu^a, Gülsen Uçarkuş^a, K. Kadir Eriş^a, Pierre Henry^b, M. Namık Çağatay^a

5 (a) Istanbul Technical University, Geological Engineering Department and EMCOL,
6 34469, Faculty of Mines, Ayazağa, İstanbul

7 (b) CEREGE (UMR7330), Aix-Marseille University, CNRS-IRD, 13330 Marseille, France

8
9 **Abstract**

10 Holocene earthquake history of the Central High Segment of the North Anatolian Fault is
11 examined here for the first time based on analysis of seismoturbidites within a 21-m-long piston
12 core recovered from the Kumburgaz Basin in the Sea of Marmara. The visual lithological
13 description combined with detailed grainsize analyses indicate that the deep basin hemipelagic
14 sediments are interrupted by 28 turbidite units during the last 6.1 cal kyrs BP. The turbidites
15 show strong segregation and a sharp boundary between a coarse basal part and overlying
16 homogenite as inferred from detailed sedimentological and geochemical data. Several
17 amalgamated turbidites are recognized by repeated fining upward sequences with no
18 intervening homogenite indicating multiple episodes of traction and deposition as a result of
19 various slope failures and turbidity currents. Each unit was possibly triggered by the same
20 earthquake event rupturing in the Sea of Marmara. The most common sedimentary feature is
21 the continuous parallel lamination that was presumably introduced by long lasting water
22 oscillations on suspended sediments due to the seiche effect. The establishment of geochemical
23 criteria and exclusive sedimentary processes distinguish earthquake triggered turbidites
24 (seismoturbidites) from other trigger factors. Moreover, such distinction allows us to evaluate

25 hydrodynamic sedimentary conditions and processes in the Kumburgaz Basin. The base of most
26 seismoturbidites are associated with a sharp increase in Mn concentration that can be explained
27 by a diagenetic enrichment of Mn at the oxic/anoxic interface of the sediments near the seafloor
28 prior to the deposition of the turbidite. An age-depth model of the studied core based on seven
29 AMS ¹⁴C ages allows precise correlation between historical earthquakes and seismoturbidites
30 in the Kumburgaz Basin. At least the latest nine of them fit well with the previously recorded
31 major earthquake events between ca. ~500 cal yrs BP and 2.5 cal kyrs BP.

32 **Keywords:** Earthquake geology, seismoturbidite, Kumburgaz Basin, Sea of Marmara, North
33 Anatolian Fault

34 **1. Introduction**

35 Earthquake-triggered gravity flow deposits have been used as a tool in subaqueous
36 paleoseismology to unravel earthquake cycles adjacent to plate boundaries and regions with
37 regular seismic activity. These deposits are studied by using various proxies in regions; the
38 North San Andreas Fault and Cascadia subduction zone (Adams, 1990; Goldfinger et al., 2003,
39 2007, 2008, 2011, 2017), New Zealand (Pouderoux et al., 2012a,b; Barnes et al., 2013), the
40 Mediterranean (Kastens and Cita, 1981; Cita et al., 1982, 1984, 1996; Kastens, 1984; Cita and
41 Aloisi, 2000; Polonia et al., 2013a, 2017), the west coast of Iberian Peninsula (Gracia et al.,
42 2000; Masson et al., 2011), and in Japan Sea (Nakajima and Kanai, 2000).

43 The term “seismoturbidite” implies triggering of the mass flow by an earthquake rather
44 than other possible mechanisms such as; storm waves, hyperpycnal flows, gas hydrate
45 dissociation, sediment overloading, volcanic eruptions and floods (Postma et al., 1988; Prior et
46 al., 1989; Nemeč, 1990; Mulder and Syvitski, 1995; Beck et al., 1996, 2007; Chapron et al.,
47 1999; Cita and Aloisi, 2000; Nakajima and Kanai, 2000; Shiki et al., 2000; Arnaud et al., 2002;
48 Goldfinger et al., 2003; Schnellmann et al., 2005; Carrillo et al., 2008). Although several criteria

49 based on core and seismic data have been proposed to distinguish seismoturbidites from
50 turbidites of other origins in submarine paleoseismological studies (Nakajima and Kanai, 2000;
51 McHugh et al., 2011; Çağatay et al., 2012; Eriş et al., 2012; Avşar et al., 2015; Goldfinger et
52 al., 2017; Polonia et al., 2017), their origin and depositional processes are still a matter of
53 debate.

54 After the devastating 1999 Izmit (Mw 7.4) and Düzce (Mw 7.2) earthquakes, submarine
55 paleoseismological studies have become crucial to constrain the earthquake recurrence history
56 of the North Anatolian Fault (NAF) in the Sea of Marmara (SoM) (Sarı and Çağatay, 2006,
57 McHugh et al., 2006, Beck et al., 2007) (Fig. 1). It is well known that the Northern Branch of
58 the North Anatolian Fault (NNAF) has generated more than 55 ($M_s > 6.8$) earthquakes in the
59 SoM region within the last two millennia (Ambraseys and Finkel, 1991, 1995; Guidoboni et al.,
60 1994; Ambraseys and Jackson, 2000; Ambraseys, 2002). These past earthquakes were the
61 dominant triggering mechanism for the failure of unconsolidated sediment on the northern shelf
62 slopes of the SoM (Sarı and Çağatay, 2006; McHugh et al., 2006; Beck et al., 2007; Çağatay et
63 al., 2012; Eriş et al., 2012; Drab et al., 2012, 2015).

64 Since the deep sedimentary sub-basins in the northern SoM are aligned along the segments of
65 the highly active dextral strike slip NNAF (Reilinger, 1997; Straub et al., 1997; McClusky et
66 al., 2000; Flerit et al., 2003; Reilinger et al., 2006) (Fig. 1), the sedimentary sequences of the
67 sub-basins have been interpreted to consist predominantly of turbidites of seismic origin
68 (McHugh et al., 2006; Sarı and Çağatay, 2006; Beck et al., 2007; Çağatay et al., 2012; McHugh
69 et al., 2014; Drab et al., 2015). These unique sedimentary units provide an important archive of
70 long-term earthquake activity. Previous models on the distribution of palaeoevents on each
71 individual segment suggest a non-periodic/quasiperiodic behavior for the NNAF in the SoM
72 (Fig. 11 and Table 3 in Drab et al., 2015; Fig. 9 in McHugh et al., 2014).

73 Establishing a reliable paleoseismological record in the SoM will allow us to better evaluate
74 the earthquake hazard risk for the region and İstanbul (~19 km north of the NNAF) (Fig. 1).
75 The Central High Segment, which crosses the Kumburgaz Basin, has not had any major
76 earthquakes at least for the last ~250 yrs (Parsons et al., 2000; Parsons, 2004; Pondard et al.,
77 2007) (Figs. 1,2). The instrumental seismicity shows sparse activity along the segment and
78 geodetic studies found a large uncertainty on the inter-seismic fault loading rate in this segment
79 (Ergintav et al., 2014; Sakic et al., 2016; Klein et al., 2017). Since the earthquake recurrence
80 intervals were not well resolved on the Central High Segment, the Kumburgaz Basin stands out
81 as an important location to study submarine paleoseismology (Fig. 2). Most of the submarine
82 paleoseismology studies in the sub-basins of the SoM were based on the cores collected in the
83 Tekirdağ, Central and Çınarcık basins (McHugh et al., 2006; Sarı and Çağatay, 2006; Beck et
84 al., 2007; Çağatay et al., 2012; McHugh et al., 2014; Drab et al., 2015). These previous studies
85 proposed some criteria to identify seismoturbidites, which still need improvements to
86 understand their own depositional conditions and processes.

87 In this study, we present detailed sedimentological and geochemical analysis of a 21-m-
88 long giant piston core recovered from the Kumburgaz Basin. Our main objective is to establish
89 reliable criteria for identifying seismoturbidites on the basis of multi-parameter proxies from
90 sedimentological and geochemical analyses. We also use ^{14}C ages to constrain an age-depth
91 model to evaluate the Late Holocene earthquake records within the piston core and relate the
92 seismoturbidites to historical earthquakes in the catalogues (Ambraseys and Finkel, 1991, 1995;
93 Guidoboni et al., 1994, 2005; Ambraseys, 2002; Altınok et al 2011).

94 **2. Oceanographic and geologic setting**

95 The SoM is located in the western part of the 1600-km long North Anatolian Fault Zone that
96 forms a 270-km long and 80-km wide intracontinental marine basin between the Mediterranean
97 and the Black Sea (Fig. 1). It is connected to the low-salinity Black Sea via the Bosphorus and

98 to the marine Aegean Sea via the Çanakkale Strait (Dardanelles). These two straits have sill
99 depths of approximately 65 and 35 m, respectively (Ryan et al., 1997; Ryan, 2007; Gökaşan et
100 al., 2008; Eriş et al., 2008). The shallow sill depths of the straits result in a modern two-layer
101 flow system in the SoM with a halocline at 25 m (Ünlüata et al., 1990; Beşiktepe et al., 1994).
102 Surface water circulation of the SoM forms an anticyclonic loop, due to the difference of water
103 level between the Mediterranean and Black sea (Beşiktepe et al., 1994). Especially during
104 summer to late autumn, surface water originating from the Black Sea flows through Bosphorus,
105 impacting surface water circulation in the SoM. Incoming Mediterranean waters via the
106 Çanakkale Strait induce bottom currents between water depths of 100 m and 500 m (Ünlüata et
107 al., 1990). Deep waters of the Kumburgaz Basin are influenced by this salty deep water current
108 (Beşiktepe et al., 1994). The surface and deep water masses in the SoM have the renewal time
109 of 4-5 months and 6-7 years, respectively (Beşiktepe et al., 1994).

110 The NAF diverges into two main branches before entering into the SoM, a northern
111 branch and a southern branch (Fig. 1). Based on GPS rates, the total slip rate of the NAF is 24-
112 26 mm/yr and the most active northern branch (NNAF) accommodates 60-80% of the total plate
113 motion (Reilinger, 1997; Straub et al., 1997; McClusky et al., 2000; Le Pichon et al., 2001,
114 2015; Armijo et al., 2002; Provost et al., 2003; Flerit et al., 2003; Şengör et al., 2005; Reilinger
115 et al., 2006; Grall et al., 2013). The NNAF exhibits a segmented submarine fault zone which
116 comprises the main İzmit, Prince's Island, Central High and Tekirdağ fault segments (Fig. 1).
117 Four deep sedimentary basins are aligned along the submerged section of the NNAF. West to
118 east, Tekirdağ (-1133 m), Central (-1268 m), and Çınarcık (-1276 m) basins are bounded by
119 two major ridges which form the Western and Central highs (Fig. 1). The Kumburgaz Basin is
120 located on the Central High with a maximum depth of 833 m (Figs. 1,2). The SoM deep basins
121 contain up to 6 km thick sediments as observed in deep seismic profiles (e.g., Carton et al.,
122 2003; Laigle et al., 2008), suggesting active subsidence.

123 3. Kumburgaz Basin: bathymetry and morphology

124 Kumburgaz Basin is located on the Central High and bisected by the Central High
125 Segment of the NNAF (Figs. 1,2). The basin is elongated in the NE-SW direction and formed
126 at a releasing bend of the NNAF (Fig. 2). Compared to deep basins of the SoM (Çınarcık,
127 Central and Tekirdağ), the Kumburgaz Basin is shallower in depth (-833 m) and smaller in size.
128 The eastern part of the basin is bounded by a submarine ridge, displaying 3.5-4 km offset with
129 a right lateral motion related to the NNAF (Armijo et al., 2002) (Figs. 1,2). Kumburgaz basin
130 is bordered by the Central Basin in the west and Çınarcık Basin in the east. The northern slope
131 (9° - 12°) of the Kumburgaz Basin which has a ~90 m shelf break, is marked by scars of old
132 submarine landslides and erosive features, most of which were probably enhanced by
133 earthquake activity along the NNAF (Fig. 2) (Görür and Çağatay, 2010; Özeren et al., 2010;
134 Çağatay et al., 2015b). The southern margin of the basin is bounded by a low-lying ridge, having
135 a minimum depth of -380 m (Fig. 1).

136 Three main submarine canyons (Fig. 2) and their tributaries are presumably the main
137 providers of turbidity currents to the Kumburgaz Basin floor. These canyons originate near the
138 continental-shelf break and extend to the base of the continental slope. The northeastern canyon
139 (NEC) is deflected by the NNAF and is the smallest of the three. The north western canyon
140 (NWC) is the longest canyon showing branching towards the shelf edge and a straight course
141 towards the base. The northern canyon (NC) and its tributaries spread with several branches
142 along the northern slope (Fig. 2). The bathymetry and the slope gradient model expose two
143 depocenters in the Kumburgaz Basin (Fig. 2). The eastern depocenter is larger and elongated
144 while the western depocenter is smaller and located at the mouth of the NWC (Fig. 2).
145 Additionally, there is a bathymetric barrier (BB) at the toe of NEC, having ca. 300 m length
146 and 75 m height (Figs. 2,3).

147 4. Methods & Instruments

148 **4.1. Core recovery and material**

149 A giant piston core CS-01 (21 m long) was recovered from ~833 m water depth in the
150 eastern depocenter of the Kumburgaz Basin during the “MARsite” Cruise by R/V Pourquoi
151 pas? (Figs. 2,3). Core recovery was performed by using a Calypso piston corer. Core location
152 was chosen by using sediment sounder (chirp) profiles (Fig. 3). The core was split into 1-meter-
153 long sections, photographed, described and sampled at Istanbul Technical University (ITU)
154 East Mediterranean Centre for Oceanography and Limnology (EMCOL). Core sections were
155 split into working and archive halves. Working halves were used for lithostratigraphic studies
156 and sampling for grain size, smear slide and radiocarbon analyses. The archive halves were
157 used for μ -XRF (X-ray Fluorescence) and Multi Sensor Core Logger (MSCL) analyses and
158 then placed in the core repository of ITU-EMCOL.

159 **4.2. μ -XRF core analysis**

160 Core CS-01 was analyzed by Itrax XRF Core Scanner (with Mo X-ray tube, at 30 kV,
161 50 mA; 1 mm resolution, 10 s for each measurement time) at ITU-EMCOL Core Analysis
162 Laboratory. The relative elemental abundances of Fe, Ca, Sr, K, and Mn were recorded as
163 counts per second (cps). Both Mn and Fe are redox sensitive elements. However, we normalized
164 Mn and Fe elements with Ca to prevent carbonate dilution effect. Mn/Ca is mainly used for
165 determination of migrating redox fronts due to the accumulation of gravity flow deposits
166 (Hofmann, 1999; Çağatay et al., 2012). Fe/Ca can display both redox sensitivity (showing
167 positive anomalies on Fe monosulfides) and detrital input. Ca and Sr are indicators of carbonate
168 content, mainly of biogenic origin in the SoM. Abundance of K is related to detrital input, and
169 correlate with fine silt and clay size minerals (e.g., illite, mica, feldspar).

170 **4.3. Physical properties and grain-size analyses**

171 The physical properties (gamma density and magnetic susceptibility) of the core were
172 measured on the archive-half at 1 cm resolution using a Geotek MSCL at the ITU-EMCOL core
173 analysis laboratory. Magnetic susceptibility (M.S.) analysis was performed by using a
174 Bartington point sensor. Positive M.S. anomalies are in general related to terrigenous input.
175 Gamma-ray density is related with density and porosity and sorting of the material. Grain-size
176 analysis of the core was performed with 5 cm sampling interval using Malvern Mastersizer
177 3000 Grain-Size Analyzer without any pretreatment due to lack of macro fossil assemblages.
178 Grain-size distribution of turbidites is determined with 0.5 cm sampling interval in order to
179 obtain higher resolution grain-size parameters (sorting and skewness). The grain-size fractions
180 (sand, silt and clay) for each seismoturbidite unit in the core were calculated according to the
181 Wentworth scale (Wentworth, 1922). Mineral composition and benthic foraminifera
182 identification in the turbidite units were made on the sieved $>63 \mu\text{m}$ fraction at 0.5 cm sampling
183 interval.

184 **4.4. Radiocarbon Analysis and Age-depth model**

185 AMS ^{14}C analyses of 7 samples were carried out at the ARTEMIS CNRS facility (Gif-
186 sur-Yvette). Hemipelagic sediment samples from beneath the mass-flow units were wet-sieved
187 and $>63 \mu\text{m}$ fractions were used to hand-pick carbonate shell material under binocular
188 microscope. Because the radiocarbon datable shell material was scarce in the samples, we also
189 included epifaunal benthic foraminifera, echinoderm spicules and occasionally bivalve shells,
190 in addition to the planktonic foraminifera. Care was taken to sample shells without evidence of
191 reworking and diagenesis. All samples were washed in distilled water and dried (at 40°C) before
192 the analysis. Results were calibrated using Calib v7.0 software with Marine13.14C calibration
193 curve and a reservoir age correction of 390 ± 85 (Sinai et al., 2000) (Table 1). Inclusion of
194 benthic and pelagic shells in the same sample would not affect the reservoir age because of the
195 negligible difference (6-7 years) between the residence time of upper and lower water masses

196 in the SoM (Beşiktepe et al., 1994). Calibrated ages were processed with R-studio using the
 197 script “bacon.r”, based on Bayesian statistics, to obtain an age-depth model for the core’s
 198 sedimentary sequence, ignoring the mass-flow units. The script created age-depth models,
 199 calculating the 95% Gaussian confidence interval around the best model (Fig. 5).

200 5. Results

201 5.1. Lithostratigraphy and chronostratigraphy

202 The studied core CS-01 includes a sedimentary succession that was deposited after the latest
 203 marine connection of the SoM, sometime between 14.7-12.5 kyrs BP (Çağatay et al., 2000,
 204 2003, 2015; Vidal et al., 2010; Eriş et al., 2011, 2012). This 21 m-long succession represents a
 205 continuous record of the last ~6.1 cal. kyrs BP (Table 1, Figs. 4, 5). and is correlated with upper
 206 part the sequence observed in 3.5 kHz seismic lines (Fig. 3).

207 Core CS-01 consists of continuous “background” hemipelagic/pelagic sediments that
 208 are interrupted by 28 turbidite layers identified by visual lithology and textural properties (Fig.
 209 4). Through the core, the ‘background’ sedimentation is slightly variable in terms of siliciclastic
 210 (clay-silt) and calcareous fractions. In the first two meters, a gradual downward change in color
 211 from brownish (oxidized mud) to olive gray is observed, and thereafter the sediment color
 212 changes to gray and then dark gray between 3 m and 15 m. The rest of the core is represented
 213 by a dark greenish gray silty clay (Fig. 4). In general, the background sediments in the core
 214 display homogenous texture without distinct variations in internal sedimentary structures. The
 215 detrital carbonate grains are commonly more abundant than the biogenic components. Fe-
 216 sulfide nodules (pyrite) and patches (iron-monosulfides) are scattered throughout the core. The
 217 fine-grained ‘background’ is locally dominated by benthic foraminifera assemblages such as
 218 *ammodiscus* sp., *textularia* sp., *spiroloculina* sp., *quiqueloculina* sp., *binoculina* sp.,
 219 *triloculina* sp., *dentalina* sp., *amphicoryna* sp., *lagena* sp., *bolivina* sp., *brizalina* sp., *bulimina*
 220 sp., *uvigerina* sp., *chilostomella* sp. and *ammonia* sp. However, turbidite-homogenite units are

221 only dominated by bivalve fragments, echinoderm spicules, *ammonia* sp., *elphidium* sp.,
222 *uvigerina* sp. and *quineloculina* sp. fossils.

223 **5.2. Sedimentological characteristics of turbidites**

224 A total of 28 turbidite units consisting of a basal coarse part and the overlying
225 homogeneous mud (homogenite) were identified lithologically and labeled as ST-1 to ST-28.
226 Their thicknesses range from 2 cm to 25 cm. The total thickness of the turbidites make up 18%
227 of the 21 m-long sedimentary succession in the core. This ratio of turbidite to background
228 hemipelagic sediment in the Kumburgaz Basin is low compared to the ratios (up to 75 %
229 turbidites) in the other SoM basins (Beck et al., 2007; Çağatay et al., 2009; Eriş et al., 2012)
230 (Fig. 1).

231 The lower boundary of the coarse basal part of the turbidites with the underlying
232 hemipelagic sediments in the Kumburgaz Basin is sharp, but commonly non-erosional. Grain-
233 size fluctuations in the coarser basal part are documented as alternations of normal and reverse
234 grading, producing the thin parallel laminations observed in the core, radiographic images and
235 grain-size distributions (Figs. 6,7). According to the classification of Folk (1980), basal units
236 of the turbidites show very poorly sorted texture (ranging between 2-3) and positively skewed
237 distribution (ranging between 0 to ~0.3) (Figs. 6,7). Smear slide microscopic observations show
238 that most sand particles have pitted surfaces. The basal part also contains a high amount of
239 fossils and fossil fragments of bivalves, echinoid spicules and benthic foraminifera relative to
240 background sediments. The abrupt lithological change between the lower coarse basal parts and
241 the upper homogeneous parts can be detected in the grain-size distribution, gamma density
242 profiles and X-ray images (Fig. 6). Some turbidites in the core are stacked on top of each other
243 without any interbedded homogenite part or hemipelagic sediments, showing the properties of
244 amalgamated turbidites (Polonia et al., 2017) (Fig. 7).

245 Homogenite part of the turbidites represents the turbidite tail deposits and identified as
246 homogenous mud in the visual description. This part consists of clay to fine silt fractions with
247 a fining upward trend in grain size. Homogenite has higher gamma density values (1.59-1.62
248 gr/cc) than the hemipelagic sediments (1.57-1.59 gr/cc) (Fig. 6). The homogenite part is marked
249 by poorly sorted (1.7-2) and positively skewed (0.1-0.3) sediments that are compatible with
250 grainsize fractions, since hemipelagic sediments are dominated by finer grain size fractions
251 (lower than 8 μm) (Fig. 6). Therefore, the overlying hemipelagic layer has comparatively better
252 sorting and uniform skewness values (Figs. 6).

253 5.3. Geochemistry

254 The μ -XRF elemental composition of turbidites in core CS-01, including Mn/Ca, Fe/Ca,
255 K, Ca and Sr, are presented in Figs. 6,7. Elemental profiles of the turbidite units show similar
256 distinct trends. The most remarkable feature is a sharp increase in Mn/Ca at the base of most
257 turbidite units. The positive Mn/Ca excursion sometimes extends in the core several centimeters
258 below the base of the turbidite layer (Fig. 6). In the case of amalgamated turbidites, a single
259 Mn/Ca peak is generally found somewhere close to the base of turbidite stack (Fig. 7) and
260 multiple Mn/Ca anomalies (Fig. 7) rarely occur.

261 The coarse basal parts of most turbidite units are associated with upward increasing μ -
262 XRF Ca and Sr counts (Figs. 6,7). Basal parts of some turbidite units are commonly depleted
263 in K compared to the homogenite parts and background sediments due to lower clay (illite)
264 content and higher carbonate content (i.e., the carbonate dilution effect) (Figs. 6,7). The
265 transition from the basal coarse part to the homogenite part of some turbidites is marked by
266 abrupt increases in K and Fe/Ca and a sharp decrease in Ca and Sr. Since geochemical
267 composition is mostly related to the sediment source, rather than the depositional process, the
268 difference between homogenite and background sediments could not be determined on the basis
269 of μ -XRF elemental changes.

270 6. Discussion

271 6.1. Triggering, deposition and sediment sources of turbidites

272 As it has been previously pointed out by many authors, there can be different triggering
273 mechanisms for mass-transport deposits including turbidites. These include seismic shaking,
274 storm waves, hyperpycnal flows, gas hydrate dissociation, sediment overloading, volcanic
275 eruptions and floods (Postma et al., 1988; Mulder and Syvitski, 1995; Beck et al., 1996; Shiki
276 et al., 2000; Goldfinger et al., 2003; Schnellmann et al., 2005). Hence, establishment of
277 sedimentological and geochemical criteria for distinguishing turbidites of seismic origin from
278 other origins has been an important objective of numerous studies.

279 The most plausible triggering mechanism for turbidites in the Kumburgaz Basin is
280 seismic shaking related to the NNAF, which is known to have produced $M > 7$ earthquakes with
281 ca. 150-250 yrs reoccurrence time (Ambraseys and Finkel, 1991, 1995; Guidoboni et al., 1994;
282 Hubert Ferrari et al., 2000; Ambraseys, 2002). Other possible triggering mechanisms such as
283 storm waves, sediment loading and hyperpycnal flows can be discounted for the Kumburgaz
284 Basin for the duration of the core's record (i.e., the last 6.1 kyrs). There is no major river input
285 on the shelf surrounding the Kumburgaz Basin, with the middle Holocene sea level stand
286 reached already ca. 6.5 kyrs BP (Fairbanks, 1989) and the shelf edge located at ca. 100 m water
287 depth was 7-8 km away from the coastline. Therefore, sediment loading and hyperpycnal flows
288 are unlikely to be a causal mechanism for triggering the mass-flow events observed in this
289 basin. With the storm wave height less than 10 m and storm base level less than 30 m in the
290 SoM (Özhan and Abdallah, 1999), storm waves are also unlikely to be a cause of mass-wasting
291 events on the shelf edge and slopes of the Kumburgaz Basin.

292 Gas hydrate dissociation as a consequence of warming during Holocene is a plausible
293 mechanism of mass-wasting in the SoM, considering the gas hydrates discovered on the

294 Western High and widespread gas emissions from the active faults in the SoM (Halbach et al.,
295 2002; Armijo et al., 2005; Géli et al., 2008; Zitter et al., 2008, 2012; Bourry et al., 2009; Ruffine
296 et al., 2017). However, observations of gas escape and its past manifestations as carbonate
297 crusts are scarce in the Kumburgaz Basin (Geli et al., 2008; Dupré et al., 2015; Çağatay et al.,
298 2017), hence gas escape from sediments is a low possibility for causing turbidity currents. The
299 two-fold division of the turbidites into a coarse basal part and a homogenite part observed in
300 the Kumburgaz Basin is taken to be indicative of seismic triggering and associated tsunami
301 events in the SoM and in some lakes (Beck et al., 1996, 2007; Chapron et al., 1999; Çağatay et
302 al., 2012; McHugh et al., 2014). As a result, we consider earthquake shaking to be the most
303 plausible mechanism to trigger turbidity currents from the shelf edge and slope to the
304 Kumburgaz Basin. This conclusion is supported by specific sedimentary structures and
305 depositional characteristics of the turbidites discussed below and their correlation with the
306 historical earthquakes presented in section 6.3.

307 Geochemical and physical proxies of seismoturbidite units in CS-01 compare well with
308 those in the other basins of the SoM (Sarı and Çağatay, 2006; McHugh et al., 2006, 2014; Beck
309 et al., 2007; Çağatay et al., 2012; Eriş et al., 2012). The Mn/Ca anomalies near the base of the
310 turbidites represent diagenetic enrichment at the oxic/anoxic interface of the sediments in a
311 basin where the bottom waters are oxic (e.g., Çağatay et al., 2004, 2012) (Figs. 6,7). This
312 boundary is presently located at ca. 10 cm below seafloor in the deep basins of the SoM
313 (Çağatay et al., 2004) but was most likely shallower and closer to the sea floor during the
314 sapropel depositional events during 12.3-5.7 and 5.4-2.7 cal. kyrs BP (Çağatay et al., 2015) in
315 the SoM. The oxic/anoxic interface migrates continuously upward during slow deposition of
316 "background" hemipelagic sediments but the deposition of a new turbidite unit causes the
317 formation of a new redox front further up in the sequence while the older front will stop
318 migrating, leaving a Mn anomaly at its final location. The elevated Ca and Sr contents in the

319 sandy basal part of the seismoturbidites are further enhanced in their uppermost parts (Figs.
320 6,7). Such enrichment is attributed to high amounts of shell material transported from the shelf
321 and upper slope areas. The shell concentration at the top of the coarse basal part occurs because
322 of late deposition due to the platy shape of the biogenic carbonate particles (Figs. 6,7). The
323 presence of *ammonia* sp., *quinqueloculina* sp., *uvigerina* sp. and *elphidium* sp. in the upper part
324 of the coarse basal layer strongly indicates infralittoral and upper circalittoral depositional
325 settings on the shelf and upper slope areas (Van Morkhoven et al., 1986; Sarı and Çağatay,
326 2006). The same faunal assemblage characterizes the homogenite parts of the seismoturbidites,
327 whereas the hemipelagic part is almost dominated by *bulimina* sp. and *bolivina* sp. This finding
328 strongly indicates the difference in origin of sediments between the homogenite and the
329 overlaying hemipelagic layers.

330 Grain-size analysis (i.e. ratio of sand, silt, clay) of the seismoturbidite units together
331 with visual observations indicate poorer sorting values (Fig. 6) which have been proposed as
332 the most significant feature for seismoturbidites (Shiki et al., 2000; Arnaud et al., 2002;
333 Goldfinger et al., 2003; Schnellmann et al., 2005; Beck et al., 2007; Carrillo et al., 2008).
334 Sorting parameter together with gamma density could explain the different depositional
335 processes and related settings between the homogenite and hemipelagic sediments (Fig. 6).
336 Considering the deposition of seismoturbidite as a result of earthquakes, settling of the
337 homogenite layer must be instantaneous compared to the hemipelagic sediments, thus, the
338 resulting grain size fractions would have formed relatively more poorly sorted sediments. This
339 likely explains higher density values of homogenites within the turbidite sequence in the
340 Kumburgaz Basin (Fig. 6). Moreover, the positive skewness within the same layer reveals that
341 the homogenite is coarser than the background sediments in Kumburgaz Basin (Fig. 6).

342 Another important feature of seismoturbidites in confined basins is the multiple sand
343 laminae commonly observed in the upper part of the coarse basal unit. Such a feature is the

344 result of long lasting water-column oscillations or “seiche” (Nakajima and Kanai, 2000; Shiki
345 et al., 2000; Sarı and Çağatay, 2006; Beck et al., 2007; Çağatay et al. 2012; Eriş et al., 2012;
346 Drab et al., 2012; McHugh et al., 2014; Polonia et al 2017). Polonia et al. (2017) suggests a
347 different model for effects of water oscillations on gravity flows. They suggest that oscillations
348 caused by earthquakes in the Ionian Sea created secondary dilute turbidity currents that
349 deposited sediments overlaying the homogenite. Furthermore, they suggest triggering of wave-
350 induced bottom currents that are also caused by the seiche effect. Based on the intensity of the
351 earthquake, distance between hypocenter and basin, and size of the water mass, internal seiche
352 can occur on the basin floor. Hence, the highly fluctuating grain size within the laminated part
353 could be generally regarded as due to oscillatory currents following an earthquake or large
354 landslide, although the hydrodynamic processes by which these oscillatory currents are
355 generated may depend on the case. Similarly, the laminated texture of the seismoturbidites in
356 the Kumburgaz Basin is most likely produced from the “to and fro” oscillating bottom currents
357 after earthquakes (Figs. 6,7).

358 Such an oscillatory mechanism in the Kumburgaz Basin may also be responsible for a
359 segregation of the bed load from the suspended load, sharpening the boundary between coarse
360 and fine-grained layers. The overlying finer part consists of silt and silt-clay size fractions,
361 where the transition zone is between the basal flow and the suspended cloud, was intensely
362 affected by seiche oscillations resulted in formation of multiple laminations (Figs. 6,7). A
363 similar depositional process was previously described by Beck et al. (2009) for Lake Annecy
364 in France, which is a much smaller basin compared to the Kumburgaz Basin. The “homogenite”
365 part overlying the coarse basal part in core CS-01 represents the mud deposited from the
366 suspended load derived from the outer shelf and slope, and the basinal sediments re-suspended
367 from the Kumburgaz Basin floor (Figs. 1, 2). The relatively uniform elemental composition as
368 inferred from XRF analysis support this conclusion. The lack of vertical changes in texture and

369 chemical composition implies deep horizontal spreading, similar to any hyperpycnal
370 depositional process in deep marine basins (Mulder et al., 1994; Mulder and Cochonat, 1996;
371 Bouma, 2000).

372 Apart from the overall physical and geochemical data discussed for the seismoturbidites
373 above, the coarse-grained lower parts, represent a coarse-tail, graded unit that is indicative of
374 low shear stress during a period of rapid sediment fall-out as a traction carpet formed at the
375 base of a turbulent suspension. The general normal grading texture in the seismoturbidite layer
376 is attributed to the waning phase of the turbidite flow (Fig. 6) (Bouma, 1962; Lowe, 1979),
377 when the energy of flow drops gradually. Whereas, grainsize grading is disturbed by
378 fluctuations based on the grainsize parameters (Figs. 6,7). This can be explained by existence
379 of seiche effect during or just after the earthquake, giving rise to strong segregation on
380 suspended particles. This kind of water column oscillations might have produced poorer sorted
381 homogenite in contrast to finer part of a classical turbidite sequence (e.g., division E; Bouma,
382 1962). Moreover, the only significant sedimentary structure in the basal part of the
383 seismoturbidite is a parallel lamination that is mostly associated with a silt dominated layer.
384 Apart from the lamination (Figs. 6,7), the lack of other internal structures defining a classical
385 Bouma turbidite sequence (Bouma, 1962; Lowe, 1979,1982; Shanmugam, 1997) could be the
386 most remarkable texture of seismoturbidites in the Kumburgaz Basin.

387 The thickness of the Kumburgaz Basin seismoturbidites range between 2 cm and 25 cm
388 (including homogenite part) (Figs. 6,7), which are commonly thinner than those reported from
389 the Tekirdağ, Central and Çınarcık basins (McHugh et al., 2006, 2014; Beck et al., 2007;
390 Çağatay et al, 2012; Eriş et al., 2012; Drab et al., 2012, 2015). This difference is likely the result
391 of several factors including the size of the basin, size of the drainage area, paleoclimate, sea
392 level, size of slope failure and the distance between the depositional basin and epicentral area.
393 During high-stand condition in the SoM after initial flooding of the shelves at 12.5 cal. kyrs

394 BP, the warm period would have decreased the stream power to generate low river sediment
395 input on the shelves (Çağatay et al., 2009; Eriş et al., 2012). Several authors also note that mass
396 transport processes and turbidity currents were more frequent and the turbidites were thicker
397 during the lacustrine stage than during the marine episode (Beck et al., 2007, 2014; McHugh et
398 al., 2008; Eriş et al., 2012). The seismoturbidites in core CS-01 were deposited during the high
399 sea level stand. They have similar elemental profiles (e.g., K, Fe/Ca, Ca, Sr) (Figs. 6,7),
400 suggesting a uniform source of the clastic fractions derived from a catchment area with
401 relatively uniform lithology, mainly the Oligocene deltaic sandstones and siltstones (Görür and
402 Okay, 1996; Okay et al., 2000; Adatepe et al., 2002).

403 We have identified 28 seismoturbidite units in the Kumburgaz Basin over the last 6.1
404 cal kyrs BP. This number is similar to that observed from the Central Basin depocenter (21
405 event in the last 5 cal. kyrs BP; McHugh et al., 2014), but more than those observed in the
406 Çınarcık Basin (Beck et al., 2007; Eriş et al., 2012). Such inconsistency in the quantity of
407 seismic events obtained from those basins is most probably due to the proximity of the basin to
408 the earthquake epicenter (Fig. 1). Other factors include, susceptibility of the slopes to mass
409 wasting, sediment storage on the shelf and slopes, and the presence of submarine canyon feeder
410 system in the basin (Fig. 2).

411 **6.2 Amalgamated Turbidites**

412 Some seismoturbidites in the Kumburgaz Basin are stacked on top of each other and as
413 such display the features of amalgamated turbidites (Nelson et al., 2012; Gutiérrez-Pastor et al.,
414 2013; Polonia et al., 2017) (Fig. 7). In such amalgamated turbidites, several fining upward
415 layers indicate multiple episodes of traction and deposition of mass-transport material
416 originating from various slope failures and transported via different submarine channels. Some
417 members of the amalgamated seismoturbidite sequences were likely triggered by the same
418 earthquake event rupturing the basin. However, in other seemingly amalgamated

419 seismoturbidites, each coarser basal part is associated with a Mn/Ca-anomaly, indicating a time
420 gap between the two events that allowed the development of new Mn/Ca-anomaly after the
421 previous event (e.g., ST-6, Fig. 7).

422 According to Polonia et al. (2017), earthquake-triggered gravity flows originating from
423 multiple sources may form amalgamated structures as stacked turbidite packages (Fig. 7).
424 Therefore, an amalgamation of seismoturbidites in the Kumburgaz Basin may have produced
425 stacked coarse layers without homogenite, since multiple gravity flows during a single
426 earthquake would not have allowed the deposition of the suspended particle cloud, that forms
427 the homogenite on the basin floor. Presence of amalgamated turbidites is detected on the core.
428 In ST-7 (Fig.7), three turbidite deposits capped with a homogenite layer suggest that these
429 turbidites might be the result of subsequent slope failures during a single earthquake, as
430 previously proposed for the Çınarcık Basin (Fig. 7) (Sarı and Çağatay 2006; Eriş et al., 2012;
431 Drab et al., 2012).

432 The stacked layers within amalgamated unit are compositionally similar in coarse
433 fraction which suggests multiple slides from the same sources. This is supported by similar
434 trends in some elemental profiles (Fe/Ca, Ca and Sr) through the seismoturbidite layers (Fig.
435 7). The catchment areas of the two main feeder canyons on the northern shelf (NC and NEC;
436 Figs. 1,2) are characterized by similar lithological composition (erosion products of Oligocene
437 siliciclastic rocks; Görür and Okay, 1996; Okay et al., 2000; Adatepe et al., 2002), so it is not
438 possible to distinguish the source of any particular seismoturbidite. It is possible that the
439 observed seismoturbidite results from a unique major mass wasting event, or from the gathering
440 of several slumps turning into coeval turbidites and channelized within three main canyons
441 around the basin (Fig. 2).

442 **6.3 Correlation of the turbidites with historical earthquakes and late Holocene** 443 **Earthquake records from Kumburgaz Basin**

444 According to the age-depth model, core CS-01 covers a period between ca. ~813 cal. a.
445 BP and ~6116 cal. a. BP (Fig. 5), and includes 28 seismoturbidite (ST) units interrupting the
446 marine hemipelagic sequence. The most recent important historical earthquakes (i.e.; AD 1766,
447 1509 and 1343) were not detected in this core, since the top ~2.5 m was not recovered. Nine of
448 the seismoturbidites are within the ~2300 years-long historical period for which earthquake
449 records are available in the published historical catalogues (e.g., Ambraseys and Finkel, 1991,
450 1995; Guidoboni et al., 1994, 2005; Ambraseys, 2002; Altınok et al 2011; Tables 2,3). Although
451 the age range of some of the seismoturbidites correspond to more than one historical
452 earthquake, we chose to select the relatively large magnitude earthquake within the age-model
453 interval, with the epicenters closest to the Kumburgaz Basin (Fig. 5, Tables 2,3). It is important
454 to note that historical earthquake catalogs can be incomplete in terms of several factors (i.e.;
455 population, local intensity of the earthquake, political circumstances, wars, distraction from
456 other natural disasters) usually affecting the records of the chronologists. Hence, we chose to
457 rely on earthquakes that are documented in several historical catalogs.

458 ST-1 is dated between 1077 AD – 817 AD (mean age is ~964 AD), and may be
459 correlated to a number of earthquakes that occurred during this interval; 1063 AD, 1010 AD,
460 989 AD, 862 AD are all documented in the catalogues as earthquakes affecting Constantinople
461 (İstanbul) region (Ambraseys and Finkel, 1991; Ambraseys, 2002; Guidoboni et al., 2005).
462 However, the 989 AD (7.2 Ms) and the 1010 AD (7.0 Ms) earthquakes are described to cause
463 more significant destruction to Constantinople compared to the other earthquakes listed above
464 and better mesh with the mean age of the ST-1. Guidoboni et al. (2005) mention that the
465 buildings including several churches and specifically the Churches of Forty Martyrs and All
466 Saints in Constantinople was damaged by the earthquake shocks of the 1010 AD. Records
467 mention about aftershocks lasting for forty days following the main event. The 989 AD
468 earthquake was reported to cause a larger scale destruction in Constantinople where houses, the

469 city walls and western side of the St. Sophia collapsed. [Guidoboni et al. \(1994\)](#) describe
470 systematic aftershocks following the 989 AD earthquake. This earthquake set up waves in the
471 sea between the provinces of Thrace to İstanbul described as tsunami waves in [Altinok et al.](#)
472 [\(2011\)](#). Based on the destruction intensity reported in the historical records and the thickness
473 of the ST-1 (the thickest in CS-01; ~ 50 cm), the 989 AD earthquake is the most likely event
474 that can be correlated with this seismoturbidite unit. Sedimentary records related to the 989 AD
475 earthquake are also documented in the Çınarcık Basin ([Drab et al., 2015](#)) (Table 3).

476 ST-2, with a calibrated age of 975 AD – 640 AD (mean: ~820 AD), can be correlated
477 with the 989 AD, 869 AD, 862 AD, 796 AD earthquakes which affected Constantinople
478 (İstanbul) and its surrounding areas ([Guidoboni et al., 1994](#); [Ambraseys, 2002](#)). Historical
479 reports describe severe damages and fatalities in Constantinople during the 862 AD and the 869
480 AD earthquakes. The 869 AD was mentioned as an earthquake that lasted for forty days and
481 forty nights (most probably aftershocks lasting 40 days); many churches collapsed including
482 the St. Mary, killing many people inside it ([Guidoboni et al., 1994](#)). The 862 AD earthquake
483 was reported to cause series of strong ground shakings bringing down the city walls of
484 Constantinople. Statue of Victory at the Golden Gate and church of St. Anne collapsed during
485 this earthquake ([Guidoboni et al., 1994](#)). The 862 and 869 AD earthquakes better fall in the
486 range of the mean age of the ST-2 and most likely represent the closest epicenters to İstanbul
487 based on the damages caused among the other earthquakes listed above.

488 ST-3 is within the age range of 963 AD – 608 AD (mean: ~796 AD). Within this interval,
489 it may correspond to the 869 AD, 862 AD, 849-851 AD, 796 AD, 740 AD earthquakes, all
490 documented within the Constantinople region ([Ambraseys and Finkel, 1991](#); [Ambraseys, 2002](#);
491 [Guidoboni et al., 2005](#)). and one of the 869 AD and 862 AD earthquakes are most likely
492 associated with the deposition of ST-2 thus we seek to understand the details of other events
493 that are listed here. The 849-851 AD is mentioned as a moderate earthquake in the catalogues

494 and the 796 AD is reported with very few details. The largest earthquake within the age range
495 of ST-3 is the 740 AD event with $M_s=7.1$ and $I=IX-XI$ (Guidoboni et al., 1994; Ambraseys,
496 2002; Altinok et al., 2011). Large scale destruction in İstanbul, İzmit and its surroundings, and
497 a tsunami affecting the coastal areas of İzmit, were reported (Altinok et al., 2011). The
498 aftershocks of this earthquake lasted almost a year (Guidoboni et al., 1994). The 740 AD may
499 have caused the deposition of ST-3 also taking into account the good fit with mean age of ST-
500 3. This event has also been observed as a distinct seismoturbidite unit in the sedimentary
501 sequences of most SoM basins (McHugh et al., 2006; Çağatay et al., 2012; Drab et al., 2015)
502 (Table 3).

503 ST-4 gives a wider age interval between 907 AD – 357 AD (mean age: ~658 AD) based
504 on the age-depth model thus it may coincide with long list of historical earthquakes affected
505 Constantinople region (862 AD, 796 AD, 740 AD, 557 AD, 554 AD, and 478-480 AD)
506 (Guidoboni et al., 1994; Ambraseys, 2002). It is rather difficult to make a more precise
507 correlation from the historical events within a ~600 age interval. Therefore, we chose to select
508 events that fits better with the mean age of the ST-4 and neglect the ones already discussed for
509 the previous seismoturbidite records. There are two major earthquakes (557 AD and 554 AD)
510 in the region that may correspond to the deposition of ST-4. The 557 AD event is described in
511 detail in many historical records as a terrible and devastating earthquake destructing many
512 churches, houses, the city walls and killing many people in Constantinople (Guidoboni et al.,
513 1994). Tremors felt for ten days and a tsunami was reported (Altinok et al., 2011). A wide
514 region including Nicomedia (İzmit) and Nicea (İzник) were affected from this earthquake
515 (Guidoboni et al., 1994). The 554 AD earthquake was felt in Constantinople (İstanbul) where
516 houses, churches and part of the walls of Constantinople were damaged or collapsed during this
517 earthquake (Ambraseys and Finkel, 1991; Guidoboni et al., 1994). ST-4 may correspond to
518 either the 554 AD or the 557 AD earthquakes. However, the 557 AD is documented as a larger

519 earthquake and may be a closer epicenter to İstanbul. Sedimentary records of the 557 AD
520 earthquake were also documented in the Central Basin (McHugh et al., 2014) (Table 3).

521 ST-5 is dated between 858 AD – 233 AD (mean age: ~578 AD) within the age-depth
522 model. The 740 AD, 557 AD, 554 AD, 542 AD, 478 AD, 447 AD earthquakes all fall into the
523 ~550 age interval (Ambraseys and Finkel, 1991; Guidoboni et al., 1994; Ambraseys, 2002).
524 The 478 AD and the 447 AD (both events are considered as I: IX) are mentioned as major
525 earthquakes that damaged Constantinople and the Marmara region in several catalogues
526 (Ambraseys and Finkel, 1991; Guidoboni et al 1994; Ambraseys, 2002; Altinok et al., 2011)
527 and Altinok et al. (2011) suggest occurrence of tsunami waves after these earthquakes. The 542
528 AD is reported with less detail in Guidoboni et al. (1994), thus either of the 478 AD and the
529 447 AD earthquakes may be the likely matches of the ST-5. There are sedimentary records also
530 dated corresponding to the 478 AD earthquake in Çınarcık Basin (Drab et al., 2015) (Table 3).

531 ST-6 has an age range between 746 AD – 169 AD (mean: ~464 AD). The earthquakes
532 documented in Constantinople region within this interval covers the 740 AD, 557 AD, 554 AD,
533 478 AD, 447 AD, 437 AD, 407 AD, 358 AD earthquakes (Guidoboni et al 1994; Ambraseys
534 and Finkel, 1991; Ambraseys, 2002). The 437 AD earthquake was described as a great
535 earthquake lasting for four months; this event was reported from one reliable source in the
536 history (Guidoboni et al 1994). The 407 AD earthquake destroyed many houses, caused
537 damage and casualties in Constantinople particularly in the coastal districts. Sea waves are
538 reported on the shores wrecking many ships (Ambraseys and Finkel, 1991). The Ottoman
539 archives confirm that many ships sunk because of a tsunami caused by an earthquake (Altinok
540 et al., 2011). There are several reports on the destructiveness of the 407 AD earthquake thus it
541 is most likely that it may correspond to ST-6. Although the 358 AD event affected
542 Constantinople, the majority of the damage was reported in the city of Nicomedia (İzmit) and

543 Nicea (İzmit). Sedimentary records are documented the 358 AD earthquake in Gulf of İzmit
544 (Çağatay et al., 2012) (Table 3) supports the distance of this event from Istanbul.

545 ST-7 has an age range of 328 AD-43 BC (mean. ~135 AD). Few chronologically
546 accurate events can be found in the historical catalogues within this time interval (the 180-181
547 AD and the 120-128 AD earthquakes). The 180-181 AD earthquake was mentioned as the third
548 catastrophe for Nicomedia (İzmit) describing a very destructive earthquake (Guidoboni et al.,
549 1994; Ambraseys, 2002). Records mention that the Emperor requested support for
550 reconstruction of the damaged regions (Guidoboni et al., 1994; Ambraseys, 2002). Another
551 major earthquake reported to destroy the greater part of Nicomedia (İzmit) together with their
552 respective districts in the 120-128 AD. The 120-128 AD and the 180-181 AD earthquakes are
553 in agreement with the mean age value of ST-7 and can most likely be associated with this
554 sedimentary record. Sedimentary traces of 180-181 AD earthquake are also dated in other cores
555 from the Gulf of İzmit (McHugh et al., 2006) (Table 3).

556 The age of ST-8 ranges between 88 AD – 206 BC (mean: ~63 BC) and may be
557 associated with the 69 AD and the 29 AD earthquakes documented in Constantinople and
558 surrounding regions (Guidoboni et al 1994; Ambraseys, 2002). The 29 AD and the 69 AD
559 earthquakes are described as damaging the Nicea (İzmit) and the Nicomedia (İzmit) regions,
560 respectively, which were the two major settlements in eastern Marmara (Bithynia) at that
561 period. Therefore, one of those can be responsible for the deposition of ST-8.

562 ST-9 has an age range of 119 BC – 458 BC (mean: ~284 BC). The 427 BC earthquake
563 described in the ancient catalogues damaging the city Perinthos (Marmara Ereğlisi), which was
564 the main settlement at the time (Guidoboni et al., 1994). The 287 BC occurred in Lysimachia
565 (around Şarköy) and mostly damaged Hellespont area (Dardanelles). It is difficult to match
566 these events precisely with ST-9 since there were no major settlement in İstanbul at that time.
567 Therefore, from this point forward the historical records provide limited information in terms

568 of damage intensities corresponding to wider areas. Either of the 287 BC and the 427 BC can
569 be correlated with ST-9.

570 The remaining 19 seismoturbidites have mean values based on the age-depth model (Table 2,
571 Fig. 5). Sedimentary section from CS-01 provide records of 28 seismoturbidite units within the
572 last ~6116 yrs suggest an average recurrence time interval of. ~220 yrs. The interval between
573 consecutive events ranges between 40 yrs to 425 yrs in Kumburgaz Basin. The average
574 earthquake recurrence interval derived from CS-01 core from Kumburgaz Basin is compatible
575 with the recurrence interval of 150-250 yrs of the NNAF based on historical records
576 (Ambraseys and Finkel, 1991, 1995; Guidoboni et al., 1994, 2005; Ambraseys and Jackson,
577 2000; Ambraseys, 2002) and the geodetic and seismological studies (Reilinger, 1997, Straub et
578 al., 1997, McClusky et al., 2000; Flerit et al., 2003; Pondard et al., 2007; Reilinger et al., 2006).
579 The recent well known earthquake sequence of the 1999 AD, 1912 AD, 1894 AD, May 1766
580 AD, August 1766 AD, 1719 AD, 1754 AD and 1509 AD ($M > 7$) earthquakes are produced by
581 the rupture of submerged segments of the NNAF (Fig.1) in the SoM (Ambraseys, 2001,2002;
582 Barka et al., 2002; Parsons, 2004; Armijo et al., 2005; Pondard et al., 2007; Uçarkuş et al.,
583 2011; McHugh et al., 2014), highlighting the consecutive earthquake cycle for the last 500 yrs
584 and supporting the recurrence time interval of 150-250 yrs.

585 7. Conclusion

586 Basins of the SoM acts as recorders of sediment input fluctuations due to tectonic activity of
587 the North Anatolian Fault. Thus, the study of seismoturbidite sequences is a critical tool to
588 evaluate earthquake recurrence intervals on such a seismically active fault zone. Our multi-
589 parameter study on a piston core (Core MRS-CS-01) from Kumburgaz Basin, is the first high
590 resolution sedimentological and geochemical study revealing the seismoturbidites deposited
591 over the last ~6.1 kyrs for this basin. Core MRS-CS-01 includes 28 turbidite units that are
592 intercalated with hemipelagic sediments. Turbidite-Homogenite units are characterized by a

593 coarse laminated sandy-silty basal part, overlaid by a seiche controlled laminated part and a
594 homogeneous mud (homogenite) cap. Based on the geochemical, physical and textural proxies
595 together with ^{14}C dating, the most probable trigger is inferred to be earthquakes. Indications of
596 earthquake triggering comprise deposition of thinly laminated deposits caused by oscillatory
597 currents and deposition from multiple gravity flow deposits (amalgamated turbidites) triggered
598 by the same or by subsequent events.

599 All 28 seismoturbidite units show similar detrital markers. Coarse laminated sand-silty basal
600 parts show high magnetic susceptibility and gamma density values due to accumulation of the
601 detrital elements (High Fe/Ca and K, low Ca and Sr content). Oscillations of current intensity,
602 presumably related to seiche effects, caused the deposition of thin laminations that result in
603 rapidly varying elemental compositions. Laminations are capped with a Ca and Sr increase
604 which is caused by the accumulation of biogenic fragments at the top of the turbidite. The
605 homogenite layer results from the deposition of the fine particle cloud sent in suspension by the
606 gravity currents, and is dominated by the clay fraction (High K) with a gradually decreasing
607 gamma density at its top. Mn/Ca anomalies are another important indicator, which is detected
608 as one or several positive spikes at the base of the seismoturbidites. These Mn/Ca anomalies
609 are interpreted as fossil redox fronts. Based on the multi-parameter analyses, we conclude that
610 the seismoturbidites of the Kumburgaz basin differ from the typical turbidite description (e.g.
611 Bouma sequence) and also presents some differences from turbidites of the other basins of SoM.
612 The seismoturbidite records from core CS-01 provide an average recurrence time interval of
613 ~ 220 yrs for the last 6.1 kyrs which is in agreement with geodetic, seismological studies and
614 historical earthquake records from the SoM. 9 out of 28 seismoturbidites from CS-01 can be
615 associated with historical earthquakes reported in the last two millennia. These frequent long-
616 term sedimentary traces (28 ST unit in ~ 6 kyrs) found in CS-01 suggest that the Kumburgaz
617 Basin has been recording earthquakes as much as other deeper basins along the NNAF in the

618 SoM. The most recent part of the sedimentary record (ca. 1200 yrs to present) is missing from
619 this core, thus it is still not known whether the 1766 AD, the 1509 AD or the 1343 AD
620 earthquakes were related to Central High Segment or not. Further core recovery and sediment
621 analysis are crucial to enlighten the correspondence of recent large earthquakes with this
622 segment to make a more precise seismic hazard assessment for İstanbul.

623 **Acknowledgements**

624 Cores were taken during MARSITECRUISE of Ifremer/Genavir R.V. *Pourquoi Pas ?*, within
625 the framework of MARSITE FP7 EU Project (Grant Agreement no.: 308417). Radiocarbon
626 dating was performed at ARTEMIS (French national radiocarbon dating facility) and funded
627 by INSU post-cruise research support program. Part of this work has been supported by
628 Bilateral ANR/TÜBITAK collaborative research project MAREGAMI (ANR-16-CE03-0010-
629 02 and Tubitak Project (116Y371). Apart of this work has been supported by ITU BAP project
630 (39273). All geochemical and sedimentological analyses were performed in ITU EMCOL
631 laboratories. We wish to thank Dursun Acar for his support during the analyses, Edouard Bard
632 and Bora Ön for their help and advice on age model construction.

633

634 **References**

- 635 Adams, J., 1990. Paleoseismicity of the Cascadia subduction zone: Evidence from turbidites
636 off the Oregon-Washington margin. *Tectonics*, 9(4), 569-583.
- 637 Aksu, A. E., Hiscott, R. N., & Yaşar, D., 1999. Oscillating Quaternary water levels of the
638 Marmara Sea and vigorous outflow into the Aegean Sea from the Marmara Sea–Black Sea
639 drainage corridor. *Marine Geology*, 153(1-4), 275-302.
- 640 Altinok, Y., Alpar, B., Özer, N., & Aykurt, H., 2011. Revision of the tsunami catalogue
641 affecting Turkish coasts and surrounding regions. *Natural Hazards and Earth System Sciences*,
642 11(2), 273.
- 643 Ambraseys, N.N., Finkel, C.F., 1991. Long term seismicity of the Istanbul and of the Marmara
644 Sea region. *Terra Nova* 3, 527–539.
- 645 Ambraseys, N.N., Finkel, C.F., 1995. The Seismicity of Turkey and Adjacent Areas-A
646 Historical Review. Eren Yayıncılık, Istanbul, pp. 1500–1800. 240 pp.
- 647 Ambraseys, N.N., Jackson, J.A., 2000. Seismicity of Sea of Marmara (Turkey) since 1500.
648 *Geophysics Journal International* 141, F1–F6.
- 649 Ambraseys, N. N. 2001. The earthquake of 1509 in the Sea of Marmara, Turkey, revisited.
650 *Bulletin of the Seismological Society of America*, 91(6), 1397-1416.
- 651 Ambraseys, N.N., 2002. The seismic activity of the Marmara Sea region over the last 2000
652 years. *Bulletin of the Seismological Society of America* 92, 1–18.
- 653 Armijo, R., Meyer, B., Navarro, S., King, G., Barka, A., 2002. Asymmetric slip partitioning in
654 the Sea of Marmara pull-apart: a clue to propagation processes of the North Anatolian Fault.
655 *Terra Nova* 14 (2), 80–86.
- 656 Armijo, R., Pondard, N., Meyer, B., Mercier de Lapinay, B., Uçarkus, G., the
657 MARMARASCARPS Cruise Party, 2005. Submarine fault scarps in the Sea of Marmara pull-
658 apart (North Anatolian Fault): implications for seismic hazard in Istanbul. *Geochemistry*,
659 *Geophysics, Geosystems* 6, 1–29.

- 660 Arnaud, F., Lignier, V., Revel, M., Desmet, M., Beck, C., Pourchet, M., Charlet, F., Trentesaux,
661 A., Tribouvillard, N., 2002. Flood and earthquake disturbance of ^{210}Pb geochronology (Lake
662 Anterne, NW Alps). *Terra Nova* 14, 225–232.
- 663 Avşar, U., Hubert-Ferrari, A., De Batist, M., Schmidt, S., & Fagel, N., 2015. Sedimentary
664 records of past earthquakes in Boraboy Lake during the last ca 600 years (North Anatolian
665 Fault, Turkey). *Palaeogeography, Palaeoclimatology, Palaeoecology*, 433, 1-9.
- 666 Barka, A., Akyuz, H. S., Altunel, E., Sunal, G., Cakir, Z., Dikbas, A., ... & Rockwell, T. 2002.
667 The surface rupture and slip distribution of the 17 August 1999 Izmit earthquake (M 7.4), North
668 Anatolian fault. *Bulletin of the Seismological Society of America*, 92(1), 43-60.
- 669 Barnes, P. M., Bostock, H. C., Neil, H. L., Strachan, L. J., & Gosling, M. 2013. A 2300-Year
670 Paleearthquake Record of the Southern Alpine Fault and Fiordland Subduction Zone, New
671 Zealand, Based on Stacked Turbidites. *Bulletin of the Seismological Society of America*,
672 103(4), 2424-2446.
- 673 Beck, C., Manalt, F., Chapron, E., Van Rensbergen, P., De Batist, M., 1996. Enhanced
674 seismicity in the early post-glacial period: evidence from the post-würm sediments of Lake
675 Annecy, Northwestern Alps. *Journal of Geodynamics* 22, 155–171.
- 676 Beck, C., Mercier de Lapinay, B., Schneider, J.L., Cremer, M., Cagatay, N., Wendenbaum, E.,
677 Boutareaoud, S., Menot, G., Schmidt, S., Webe, O., Eris, K., Armijo, R., Meyer, B., Pondard,
678 N., Gutcher, M.A., Turon, J.L., Labeyrie, L., Cortijo, E., Gallet, Y., Bouquerel, H., Gorur, N.,
679 Geravis, A., Castera, M.H., Londeix, L., de Resseguier, A., Jaouen, A., 2007. Late Quaternary
680 co-seismic sedimentation in the Sea of Marmara's deep basins. *Sedimentary Geology* 199, 65–
681 89.
- 682 Beck, C., 2009. Late Quaternary lacustrine paleo-seismic archives in north-western Alps:
683 examples of earthquake-origin assessment of sedimentary disturbances. *Earth Science Review*
684 96, 327–344.
- 685 Beşiktepe, Ş. T., Sur, H. I., Özsoy, E., Latif, M. A., Oğuz, T., & Ünlüata, Ü., 1994. The
686 circulation and hydrography of the Marmara Sea. *Progress in Oceanography*, 34(4), 285-334.

- 687 Bouma A. H., 1964. Turbidites. In: Bouma AH, Brouwer A (eds) Turbidites. Developments in
688 sedimentology, vol 3. Elsevier, Amsterdam, pp 247–256. doi:10.1016/S0070-4571(08)70967-
689 1.
- 690 Bouma, A. H., 2000. Coarse-grained and fine-grained turbidite systems as end member models:
691 applicability and dangers. *Marine and Petroleum Geology*, 17(2), 137-143.
- 692 Bourry, C., Chazallon, B., Charlou, J. L., Donval, J. P., Ruffine, L., Henry, P., ... & Moreau,
693 M., 2009. Free gas and gas hydrates from the Sea of Marmara, Turkey: Chemical and structural
694 characterization. *Chemical Geology*, 264(1-4), 197-206.
- 695 Çağatay, N., Görür, N., Algan, O., Eastoe, C. J., Tchapylyga, A., Ongan, D., ... & Kuscu, I.,
696 2000. Late Glacial-Holocene paleoceanography of the Marmara Sea: timing of connections
697 with the Mediterranean and the Black Seas. *Marine Geology*, 167, 191-206.
- 698 Çağatay, M. N., Borowski, W. S., & Ternois, Y. G., 2001. Factors affecting the diagenesis of
699 Quaternary sediments at ODP Leg 172 sites in western North Atlantic: evidence from pore
700 water and sediment geochemistry. *Chemical Geology*, 175(3-4), 467-484.
- 701 Çağatay, M. N., Görür, N., Polonia, A., Demirbağ, E., Sakıncı, M., Cormier, M. H., ... & Eriş,
702 K., 2003. Sea-level changes and depositional environments in the Izmit Gulf, eastern Marmara
703 Sea, during the late glacial–Holocene period. *Marine Geology*, 202(3-4), 159-173.
- 704 Çağatay, M.N., Özcan, M., Güngör, E., 2004. Pore water and sediment geochemistry in the
705 Marmara Sea (Turkey): early diagenesis and diffusive fluxes. *Geochemistry: Exploration,
706 Environment, Analysis* 4, 213–225.
- 707 Çağatay, M. N., Görür, N., Flecker, R., Sakıncı, M., Tünoğlu, C., Ellam, R., ... & Dikbaş, A.,
708 2006. Paratethyan–Mediterranean connectivity in the Sea of Marmara region (NW Turkey)
709 during the Messinian. *Sedimentary Geology*, 188, 171-187.
- 710 Çağatay, M. N., Eriş, K., Ryan, W. B. F., Sancar, Ü., Polonia, A., Akçer, S., ... & Bard, E.,
711 2009. Late Pleistocene–Holocene evolution of the northern shelf of the Sea of Marmara. *Marine
712 Geology*, 265(3-4), 87-100.

- 713 Çağatay, M.N., Erel, L., Bellucci, L.G., Polonia, A., Gasperini, L., Eris, K., Sancar, Ü., Biltekin,
714 D., Uçarkus, G., Ülgen, U.B., Damci, E., 2012. Sedimentary earthquake records in the Izmit
715 Gulf, Sea of Marmara, Turkey. *Sedimentary Geology* 282, 347–359.
716 <http://dx.doi.org/10.1016/j.sedgeo.2012.10.001>.
- 717 Çağatay, M. N., Geli, L., Gasperini, L., Henry, P., Gürbüz, C., & Görür, N., 2015. Seafloor
718 observations and observatory activities in the Sea of Marmara. In *SEAFLOOR*
719 *OBSERVATORIES* (pp. 59-79). Springer, Berlin, Heidelberg.
- 720 Çağatay, M. N., Wulf, S., Sancar, Ü., Özmaral, A., Vidal, L., Henry, P., ... & Gasperini, L.,
721 2015. The tephra record from the Sea of Marmara for the last ca. 70 ka and its
722 palaeoceanographic implications. *Marine Geology*, 361, 96-110.
- 723 Çağatay, M. N., Yıldız, G., Bayon, G., Ruffine, L., & Henry, P., 2017. Seafloor authigenic
724 carbonate crusts along the submerged part of the North Anatolian Fault in the Sea of Marmara:
725 Mineralogy, geochemistry, textures and genesis. *Deep Sea Research Part II: Topical Studies in*
726 *Oceanography*.
- 727 Carrillo, E., Beck, C., Audemard, F.A., Moreno, E., Ollarves, R., 2008. Disentangling Late
728 Quaternary climatic and seismo-tectonic controls on Lake Mucubaji sedimentation (Merida
729 Andes, Venezuela). *Palaeogeography Palaeoclimatology Palaeoecology* 259, 284–300.
- 730 Carton, H., 2003. Structure of the Cinarcik Basin (eastern Marmara Sea) from densely-spaced
731 multi-channel reflection profiles. *Lithos Science Report*.
- 732 Chapron, E., Beck, C., Pouchet, M., Deconninck, J.F., 1999. 1822 earthquake-triggered
733 homogenite in Lake Le Bouget (NW Alps). *Terra Nova* 11, 86–92.
- 734 Cita, M.B., Bossio, A., Colombo, A., Gnaccolini, M., Salvatorini, G., Broglia, C.,
735 Camerlenghi, A., Catrullo, D., Clauzon, G., Croce, M., Giambastiani, M., Kastens, K.A.,
736 Malinverno, A., McKoy, F.W., Parisi, E., 1982. Sedimentation in the Mediterranean Ridge
737 Cleft (DSDP Site 126). *Member of Society of Geology, Italy* 24, 427–442.
- 738 Cita, M.B., Beghi, C., Camerlenghi, A., Kastens, K.A., McKoy, F.W., Nosetto, A., Parisi, E.,
739 Scolari, F., Tomadin, L., 1984. Turbidites and megaturbidites from the Herodotus Abyssal Plain
740 (Eastern Mediterranean) unrelated to seismic events. *Marine Geology* 55, 79–101.

- 741 Cita, M.B., Carmerlenghi, A., Rimoldi, B., 1996. Deep-sea tsunami deposits in the eastern
742 Mediterranean: new evidence and depositional models. *Sedimentary Geology* 104, 155–173.
- 743 Cita, M.B., Aloisi, G., 2000. Deep-sea tsunami deposits triggered by the explosion of Santorini
744 (3500 a BP), Eastern Mediterranean. *Sedimentary Geology* 135, 181–203.
- 745 Drab, L., Hubert-Ferrari, A., Schmidt, S., Martinez, P., 2012. The earthquake record in the
746 western part of the Sea of Marmara, Turkey. In: Pantosi, D. (Ed.), *Natural Hazards and Earth
747 System Sciences, Special Issue “Subaqueous Paleoseismology”*, pp. 1235–1254.
748 <http://dx.doi.org/10.5194/nhess-12-2012>.
- 749 Drab, L., Hubert-Ferrari, A., Schmidt, S., Martinez, P., Carlut, J., & El Ouahabi, M., 2015.
750 Submarine earthquake history of the Çınarcık segment of the North Anatolian Fault in the
751 Marmara Sea, Turkey. *Bulletin of the Seismological Society of America*, 105(2A), 622-645.
- 752 Ergintav, S., Reilinger, R. E., Çakmak, R., Floyd, M., Cakir, Z., Doğan, U., ... & Özener, H.
753 2014. Istanbul's earthquake hot spots: Geodetic constraints on strain accumulation along faults
754 in the Marmara seismic gap. *Geophysical Research Letters*, 41(16), 5783-5788.
- 755 Eriş K.K., Ryan WBF, Çağatay MN, Sancar U, Lericolais G, Ménot G, Bard E., 2008. Reply
756 to comment on “The timing and evolution of the post-glacial transgression across the Sea of
757 Marmara shelf south of İstanbul” by Hiscott et al. *Marine Geology* 248:228–236
- 758 Eriş, K. K., Çağatay, M. N., Akçer, S., Gasperini, L., & Mart, Y., 2011. Late glacial to Holocene
759 sea-level changes in the Sea of Marmara: new evidence from high-resolution seismics and core
760 studies. *Geo-Marine Letters*, 31(1), 1-18.
- 761 Eriş, K.K., Çağatay, N., Beck, C., Mercier de Lepinay, B., Campos, C., 2012. Late-Pleistocene
762 to Holocene sedimentary fills of the Cınarcık Basin of the Sea of Marmara. *Sedimentary
763 Geology* 281, 151–165.
- 764 Fairbanks, R. G., 1989. A 17,000-year glacio-eustatic sea level record: influence of glacial
765 melting rates on the Younger Dryas event and deep-ocean circulation. *Nature*, 342(6250), 637.

- 766 Flerit, F., Armijo, R., King, G. C. P., Meyer, B., & Barka, A., 2003. Slip partitioning in the Sea
767 of Marmara pull-apart determined from GPS velocity vectors. *Geophysical Journal*
768 *International*, 154(1), 1-7.
- 769 Géli, L., Henry, P., Zitter, T., Dupré, S., Tryon, M., Çağatay, M.N., de Lépinay, B., Mercier,
770 Le Pichon, X., Sengör, A.M.C., Görür, N., Natalin, B., Uçarkus, G., Özeren, S., Volker, D.,
771 Gasperini, L., Burnard, P., Bourlange, S., the Marnaut Scientific, Party, 2008. Gas emissions
772 and active tectonics within the submerged section of the North Anatolian Fault zone in the Sea
773 of Marmara. *Earth and Planetary Science Letters* 274 (1–2), 34–39.
- 774 Gökaşan, E., Ergin, M., Özyalvaç, M., Sur, H. İ., Tur, H., Görüm, T., ... & Türker, A., 2008.
775 Factors controlling the morphological evolution of the Çanakkale Strait (Dardanelles, Turkey).
776 *Geo-Marine Letters*, 28(2), 107-129.
- 777 Goldfinger, C., Nelson, C.H., Johnson, J.E., 2003. Holocene earthquake records from the
778 Cascadia subduction zone and northern San Andreas fault based on precise dating of offshore
779 turbidites. *Annual Review of Earth and Planetary Sciences* 31, 555–577.
- 780 Goldfinger, C., Morey, A.E., Nelson, C.H., Gutierrez-Pastor, J., Johnson, J.E., et al., 2007.
781 Rupture lengths and temporal history of significant earthquakes on the offshore and north coast
782 segments of the northern San Andreas Fault based on turbidite stratigraphy. *Earth and Planetary*
783 *Science Letters* 254, 9–27.
- 784 Goldfinger, C., Grijalva, K., Burgmann, K., Morey, A., Johnson, J.E., Nelson, C.H., Gutiérrez-
785 Pastor, J., Karabanov, E., Patton, J., Gracia, E., 2008. Late Holocene rupture of the northern
786 San Andreas Fault and possible stress linkage to the Cascadia Subduction Zone. *Seismological*
787 *Society of America, Bulletin* 98, 861–899.
- 788 Goldfinger, C., 2011. Submarine paleoseismology based on turbidite records. *Annual Review*
789 *of Marine Science* 3, 35–66.
- 790 Goldfinger, C., Galer, S., Beeson, J., Hamilton, T., Black, B., Romsos, C., ... & Morey, A.,
791 2017. The importance of site selection, sediment supply, and hydrodynamics: A case study of
792 submarine paleoseismology on the Northern Cascadia margin, Washington USA. *Marine*
793 *Geology*, 384, 4-46.

- 794 Görür, N., & Okay, A. I. 1996. A fore-arc origin for the Thrace Basin, NW Turkey. *Geologische*
795 *Rundschau*, 85(4), 662-668.
- 796 Görür, N., & Çağatay, M. N., 2010. Geohazards rooted from the northern margin of the Sea of
797 Marmara since the late Pleistocene: a review of recent results. *Natural hazards*, 54(2), 583-603.
- 798 Gracia, E., Vizcaino, A., Escutia, C., Asioi, A., Rodes, A., Pallas, R., Garcia-Orellana, J.,
799 Lebreiro, S., Goldfinger, C., 2010. Holocene earthquake records offshore Portugal (SW Iberia):
800 testing turbidite paleoseismology in a slow-convergence margin. *Quaternary Science Reviews*
801 29, 1156–1172.
- 802 Grall, C., Herny, P., Thomas, Y., Westbrook, G.K., Çağatay, M.N., Marsset, B., Saritas, H.,
803 Çifci, G., Geli, L., 2013. Slip rate estimations along the western segment of the Main Marmara
804 Fault over the last 405–490 ka by correlating mass transport deposits. *Tectonics* 32, 1–15.
- 805 Guidoboni, E., Comastri, A., Traina, G., 1994. *Catalogue of Ancient Earthquakes in the*
806 *Mediterranean Area up to 10th Century*. INGV-SGA, Bologna. 504 pp.
- 807 Guidoboni, E., Comastri, A., 2005. *Catalogue of Earthquakes and Tsunamis in the*
808 *Mediterranean Area from 11th to the 15th Century*. INGV-SGA, Bologna. 1057 pp.
- 809 Halbach, P., Kuşçu, İ., Inthorn, M., Kuhn, T., Pekdeğer, A., & Seifert, R., 2002. Methane in
810 sediments of the deep Marmara Sea and its relation to local tectonic structures. In *Integration*
811 *of Earth Science Research on the Turkish and Greek 1999 Earthquakes* (pp. 71-85). Springer,
812 Dordrecht.
- 813 Hofmann, B. A., 1999. *Geochemistry of natural redox fronts-a review*. Nagra.
- 814 Houghton, P.D.V., 1994. Deposits of deflected or ponded turbidity currents, Sorbas Basin,
815 southeast Spain. *Journal of Sedimentary Research* A64, 233–246.
- 816 Hubert-Ferrari, A., Barka, A., Jacques, E., Nalbant, S. S., Meyer, B., Armijo, R., ... & King, G.
817 C., 2000. Seismic hazard in the Marmara Sea region following the 17 August 1999 Izmit
818 earthquake. *Nature*, 404(6775), 269.
- 819 Kastens, K., Cita, M.B., 1981. Tsunami-induced sediment transport in the abyssal
820 Mediterranean Sea. *Geological Society of America Bulletin* 119, 151–165.

- 821 Kastens, K.A., 1984. Earthquakes as a triggering mechanism for debris flows and turbidites on
822 the Calabrian Ridge. *Marine Geology* 55, 13–33.
- 823 Klein, E., Duputel, Z., Masson, F., Yavasoglu, H., & Agram, P. 2017. Aseismic slip and
824 seismogenic coupling in the Marmara Sea: What can we learn from onland geodesy?.
825 *Geophysical Research Letters*, 44(7), 3100-3108.
- 826 Laigle, M., Becel, A., de Voogd, B., Hirn, A., Taymaz, T., & Ozalaybey, S. 2008. A first deep
827 seismic survey in the Sea of Marmara: Deep basins and whole crust architecture and evolution.
828 *Earth and Planetary Science Letters*, 270(3-4), 168-179.
- 829 Le Pichon, X., Şengör, A.M.C., Demirbağ, E., Rangin, C., Imren, C., Armijo, R., Görür, N.,
830 Çağatay, N., de Lepinay, B.M., Meyer, B., Saatçılar, R., Tok, B., 2001. The active main
831 Marmara fault: comparative anatomy of a continental transform fault in a marine setting. *Earth*
832 *and Planetary Science Letters* 192, 595–616.
- 833 Le Pichon, X., Şengör, A. C., Kende, J., İmren, C., Henry, P., Grall, C., & Karabulut, H., 2015.
834 Propagation of a strike-slip plate boundary within an extensional environment: the westward
835 propagation of the North Anatolian Fault. *Canadian Journal of Earth Sciences*, 53(11), 1416-
836 1439.
- 837 Lowe, D.R. 1979. Sediment gravity flows: their classification and some problems of application
838 to natural flows and deposits. In: Doyle, L.J. and Pilkey, O.H. (Eds.), *Geology of Continental*
839 *Slopes*. Society of Economic Paleontologists and Mineralogists, Special Publication 27, p. 75-
840 82.
- 841 Lowe, D. R., 1982. Sediment gravity flows: II Depositional models with special reference to
842 the deposits of high-density turbidity currents. *Journal of Sedimentary Research*, 52(1).
- 843 Major, C., Ryan, W., Lericolais, G., & Hajdas, I., 2002. Constraints on Black Sea outflow to
844 the Sea of Marmara during the last glacial–interglacial transition. *Marine Geology*, 190(1-2),
845 19-34.
- 846 Masson, D.G., Arzola, R.G., Wynn, R.B., Hunt, J.E., Weaver, P.P.E., 2011. Seismic triggering
847 of landslides and turbidity currents offshore Portugal. *Geochemistry, Geophysics, Geosystems*
848 12, 1–19. <http://dx.doi.org/10.1029/2011GC003839>.

- 849 McClusky, S., Bassalanian, S., Barka, A., Demir, C., Ergintav, S., Georgiev, I., Gurkan,
850 Hamburger, O.M., Hurst, K., Hans-Gert, H.-G., Karstens, K., Kekelidze, G., King, R., Kotzev,
851 V., Lenk, O., Mahmoud, S., Mishin, A., Nadariya, M., Ouzounis, A., Paradissis, D., Peter, Y.,
852 Prilepin, M., Relinger, R., Sanli, I., Seeger, H., Tealeb, A., Toksoz, M.N., Veis, G., 2000.
853 Global Positioning System constraints on plate kinematics and dynamics in the eastern
854 Mediterranean and Caucasus. *Journal of Geophysical Research* 105 (B3), 5695–5719.
- 855 McHugh, C.M.G., Seeber, L., Cormier, M.-H., Dutton, J., Çağatay, N., Polonia, A., Ryan,
856 W.B.F., Görür, N., 2006. Submarine earthquake geology along the North Anatolia Fault in the
857 Marmara Sea, Turkey: a model for transform basin sedimentation. *Earth and Planetary Science*
858 *Letters* 248, 661–684.
- 859 McHugh, C. M., Gurung, D., Giosan, L., Ryan, W. B., Mart, Y., Sancar, U., ... & Cagatay, M.
860 N., 2008. The last reconnection of the Marmara Sea (Turkey) to the World Ocean: a
861 paleoceanographic and paleoclimatic perspective. *Marine Geology*, 255(1-2), 64-82.
- 862 McHugh, C.M., Seeber, L., Braudy, N., Cormier, M.-H., Davis, M.B., Diebold, J.B.,
863 Dieudonne, N., Douilly, R., Gulick, S.P.S., Hornbach, M.J., Johnson III, H.E., Ryan, K.M.,
864 Sorlien, C.C., Steckler, M.S., Symithe, S.J., Templeton, J., 2011. Offshore sedimentary effects
865 of the 12 January 2010 Haiti earthquake. *Geology* 39, 723–726.
- 866 McHugh, C. M., Braudy, N., Çağatay, M. N., Sorlien, C., Cormier, M. H., Seeber, L., & Henry,
867 P., 2014. Seafloor fault ruptures along the North Anatolia Fault in the Marmara Sea, Turkey:
868 Link with the adjacent basin turbidite record. *Marine Geology*, 353, 65-83.
- 869 Mulder, T., Tisot, J. P., Cochonat, P., & Bourillet, J. F., 1994. Regional assessment of mass
870 failure events in the Baie des Anges, Mediterranean Sea. *Marine Geology*, 122(1-2), 29-45.
- 871 Mulder, T., Syvitski, J.P.M., 1995. Turbidity currents generated at river mouths during
872 exceptional discharges to the world oceans. *Journal of Geology* 103, 285–299.
- 873 Mulder, T., & Cochonat, P., 1996. Classification of offshore mass movements. *Journal of*
874 *Sedimentary research*, 66(1).

- 875 Nakajima, T., Kanai, Y., 2000. Sedimentary features of seismoturbidites triggered by the 1983
876 and older historical earthquakes in the eastern margin of the Japan Sea. *Sedimentary Geology*
877 135, 1–19.
- 878 Nemec, W., 1990. Aspect of sediment movement on step delta slope. In: Colella, A., Prior, D.B.
879 (Eds.), *Coarse Grained Deltas*. International Association of Sedimentologists Special
880 Publication, 10. Blackwell, Oxford, pp. 29–74.
- 881 Okay, A. İ., Kaşlılar-Özcan, A., Imren, C., Boztepe-Güney, A., Demirbağ, E., & Kuşçu, İ.,
882 2000. Active faults and evolving strike-slip basins in the Marmara Sea, northwest Turkey: a
883 multichannel seismic reflection study. *Tectonophysics*, 321(2), 189-218.
- 884 Özeren, M. S., Çağatay, M. N., Postacıoğlu, N., Şengör, A. C., Görür, N., & Eriş, K., 2010.
885 Mathematical modelling of a potential tsunami associated with a late glacial submarine
886 landslide in the Sea of Marmara. *Geo-Marine Letters*, 30(5), 523-539.
- 887 Özhan, E., & Abdalla, S., 2002. Türkiye Kıyıları için Rüzgar ve Derin Deniz Dalga Atlası. Kıyı
888 Alanları Yönetimi Türk Milli Komitesi, Ankara.
- 889 Parsons, T.S., Toda, T.S., Stein, R.S., Barka, A., Dietrich, J.H., 2000. Heightened odds of large
890 earthquakes near Istanbul, an interaction-based probability calculation. *Science* 288, 661–665.
- 891 Parsons, T., 2004. Recalculated probability of $M > 7$ earthquakes beneath the Sea of Marmara.
892 *Journal of Geophysical Research* 109. <http://dx.doi.org/10.1029/2003JB002667>.
- 893 Pickering, K.T., Hiscott, R.N., 1985. Contained (reflected) turbidity currents in the Middle
894 Ordovician Cloridorme Formation, Quebec, Canada: an alternative to the antidune hypothesis.
895 *Sedimentology* 32, 373–394.
- 896 Polonia, A., Panieri, G., Gasperini, L., Gasparotto, G., Bellucci, L.G., Torelli, L., 2013a.
897 Turbidite paleoseismology in the Calabrian Arc subduction complex (Ionian Sea).
898 *Geochemistry, Geophysics, Geosystems* 14, 112–140.
899 <http://dx.doi.org/10.1029/2012GC004402>

- 900 Polonia, A., Nelson, C. H., Romano, S., Vaiani, S. C., Colizza, E., Gasparotto, G., & Gasperini,
901 L., 2017. A depositional model for seismo-turbidites in confined basins based on Ionian Sea
902 deposits. *Marine Geology*, 384, 177-198.
- 903 Pondard, N., Armijo, R., King, G. C., Meyer, B., & Flerit, F., 2007. Fault interactions in the
904 Sea of Marmara pull-apart (North Anatolian Fault): earthquake clustering and propagating
905 earthquake sequences. *Geophysical Journal International*, 171(3), 1185-1197.
- 906 Postma, G., Babic, L., Zupanic, J., Roe, S.L., 1988. Delta-front failure and associated bottomset
907 deformation in a marine, gravelly Gilbert-type delta. In: Nemeč, N., Steel, R.J. (Eds.), *Fan*
908 *Deltas: Sedimentology and Tectonic Settings*. Blackie, Glasgow & London, pp. 91–102.
- 909 Pouderoux, H., Proust, J.N., Lamarche, G., Orpin, A., Neil, H., 2012a. Deep-sea sedimentation
910 along the Hikurangi subduction margin (New Zealand) since the Last Glacial Maximum:
911 characterisation, timing and origin of turbidites. *Marine Geology* 295e298, 51-76.
- 912 Pouderoux, H., Lamarche, G., Proust, J.-N., 2012b. Building a 18 000-year-long
913 paleoearthquake record from detailed deep-sea turbidite characterisation in Poverty Bay, New
914 Zealand. *Natural Hazards and Earth System Sciences*, 12, 1-25.
- 915 Prior, D.B., Suhayda, J.N., Lu, N.Z., Bornhold, B.D., Keller, G.H., Wiseman, W.J., Wright,
916 L.D., Yang, Z.S., 1989. Storm wave reactivation of a submarine landslide. *Nature* 341, 47–50.
- 917 Provost, A. S., Chéry, J., & Hassani, R., 2003. 3D mechanical modeling of the GPS velocity
918 field along the North Anatolian fault. *Earth and Planetary Science Letters*, 209(3-4), 361-377.
- 919 Reilinger, R. E., McClusky, S. C., Oral, M. B., King, R. W., Toksoz, M. N., Barka, A. A., ... &
920 Sanli, I., 1997. Global Positioning System measurements of present-day crustal movements in
921 the Arabia-Africa-Eurasia plate collision zone. *Journal of Geophysical Research: Solid Earth*,
922 102(B5), 9983-9999.
- 923 Reilinger, R., McClusky, S., Vernant, P., Lawrence, S., Ergintav, S., Cakmak, R., ... &
924 Nadariya, M., 2006. GPS constraints on continental deformation in the Africa-Arabia-Eurasia
925 continental collision zone and implications for the dynamics of plate interactions. *Journal of*
926 *Geophysical Research: Solid Earth*, 111(B5).

- 927 Ruffine, L., Donval, J. P., Croguennec, C., Burnard, P., Lu, H., Germain, Y., ... & Madre, D.,
928 2017. Multiple gas reservoirs are responsible for the gas emissions along the Marmara fault
929 network. *Deep Sea Research Part II: Topical Studies in Oceanography*.
- 930 Ryan, W. B., Pitman III, W. C., Major, C. O., Shimkus, K., Moskalenko, V., Jones, G. A., ... &
931 Yüce, H., 1997. An abrupt drowning of the Black Sea shelf. *Marine Geology*, 138(1-2), 119-
932 126.
- 933 Ryan, W. B., 2007. Status of the Black Sea flood hypothesis. In *The Black Sea Flood Question:
934 Changes in Coastline, Climate, and Human Settlement* (pp. 63-88). Springer, Dordrecht.
- 935 Sakic, P., Piete, H., Ballu, V., Royer, J. Y., Kopp, H., Lange, D., ... & Henry, P. 2016. No
936 significant steady state surface creep along the North Anatolian Fault offshore Istanbul: Results
937 of 6 months of seafloor acoustic ranging. *Geophysical Research Letters*, 43(13), 6817-6825.
- 938 Sarı, E., Çağatay, M.N., 2006. Turbidities and their association with past earthquakes in the
939 deep Çınarcık Basin of the Marmara Sea. *Geo-Marine Letters* 26, 69–76.
- 940 Schnellmann, M., Flavio, S.A., Domenico, G., Judith, A.M., 2005. Mass movement induced
941 fold-and-thrust belt structures in unconsolidated sediments in Lake Lucerne (Switzerland).
942 *Sedimentology* 52, 271–289.
- 943 Şengör, A.M.C., Tüysüz, O., İmren, C., Sakıncı, M., Eyidoğan, H., Görür, N. Le, Pichon, X.,
944 Rangin, C., 2005. The North Anatolian Fault: a new look. *Annual Review of Earth and
945 Planetary Sciences* 33, 37–112.
- 946 Shanmugam, G., 1997. The Bouma sequence and the turbidite mind set. *Earth-Science
947 Reviews*, 42(4), 201-229.
- 948 Shiki, T., Kumon, F., Inouchi, Y., Kontani, Y., Sakamoto, T., Tateishi, M., Matsubara, H.,
949 Fukuyama, K., 2000. Sedimentary features of the seismo-turbidites, Lake Biwa, Japan.
950 *Sedimentary Geology* 135, 37–50.
- 951 Siani, G., Paterne, M., Arnold, M., Bard, E., Metivier, B., Tisnerat, N., Bassinot, F., 2000.
952 Radiocarbon reservoir ages in the Mediterranean Sea and Black Sea. *Radiocarbon* 42, 271–280.

- 953 Straub, C., Kahle, H.-G., and Schindler, C., 1997. GPS and geologic estimates of the tectonic
 954 activity in the Marmara Sea region, NW Anatolia: *Journal of Geophysical Research*, v. 102, p.
 955 27,587–27,601.
- 956 Uçarkuş, G., 2010. Active Faulting and Earthquake Scarps a Long the North Anatolian Fault in
 957 The Sea of Marmara (Doctoral dissertation, Avrasya Yer Bilimleri Enstitüsü).
- 958 Uçarkuş, G., Çakır, Z., & Armijo, R. 2011. Western termination of the Mw 7.4, 1999 İzmit
 959 Earthquake rupture: Implications for the expected large earthquake in the Sea of Marmara.
 960 *Turkish Journal of Earth Sciences*, 20, 379-394.
- 961 Ünlülata, Ü., Oğuz, T., Latif, M. A., & Özsoy, E., 1990. On the physical oceanography of the
 962 Turkish Straits. In *The physical oceanography of sea straits* (pp. 25-60). Springer, Dordrecht.
- 963 Van Morkhoven, F. P., Berggren, W. A., Edwards, A. S., & Oertli, H. J. 1986. Cenozoic
 964 cosmopolitan deep-water benthic foraminifera (Vol. 11). *Elf Aquitaine*.
- 965 Vidal, L., Menot, G., Joly, C., Bruneton, H., Rostek, F., Çağatay, M. N., ... & Bard, E. (2010).
 966 Hydrology in the Sea of Marmara during the last 23 ka: implications for timing of Black Sea
 967 connections and sapropel deposition. *Paleoceanography*, 25(1).
- 968 Wentworth, C. K., 1922. A scale of grade and class terms for clastic sediments. *The journal of*
 969 *geology*, 30(5), 377-392.
- 970 Zitter, T. A. C., Henry, P., Aloisi, G., Delaygue, G., Çağatay, M. N., De Lepinay, B. M., ... &
 971 Wallmann, K., 2008. Cold seeps along the main Marmara Fault in the Sea of Marmara (Turkey).
 972 *Deep Sea Research Part I: Oceanographic Research Papers*, 55(4), 552-570.
- 973 Zitter, T. A. C., Grall, C., Henry, P., Özeren, M. S., Çağatay, M. N., Şengör, A. M. C., ... &
 974 Géli, L., 2012. Distribution, morphology and triggers of submarine mass wasting in the Sea of
 975 Marmara. *Marine Geology*, 329, 58-74.

976 **Figure Captions**

- 977 **Fig 1.** Location of the study and tectonic setting. A) Inset map shows current tectonic setting of
 978 Turkey and surroundings. B) High Resolution Multi-Beam Bathymetry Map of the Sea of

979 Marmara (CB: Central Basin, CiB; Çınarcık Basin, CH: Central High, GI: Gulf of İzmit, KB:
 980 Kumburgaz Basin, TB: Tekirdağ Basin, WH: Western High) (Revised from Uçarkuş, 2010).
 981 Black lines represent the faults. Yellow box indicates the location of the Kumburgaz Basin (Fig.
 982 2). Transparent lines represent Tekirdağ, Central High, Prince's Island and İzmit segments of
 983 the NNAF with blue, red, green and yellow colors respectively. Dashed black line represents
 984 the location of Constantinople.

985 **Fig 2.** Detailed bathymetry map of the Kumburgaz Basin and surroundings, showing locations
 986 of core CS-01 (yellow dot) and seismic reflection profile (Fig. 3) (red line). Faults are indicated
 987 with black lines. The main submarine canyons and depocenter in the basin are clearly shown in
 988 the inset map obtained by a slope gradient. (NWC: Northwestern Canyon, NC: Northern
 989 Canyon, NEC: Northeastern Canyon, WD: Western Depocenter, ED: Eastern Depocenter
 990 respectively).

991 **Fig 3.** Seismic reflection profile P02 from the Kumburgaz Basin, showing the main depositional
 992 units along the basin floor. Two different units are differentiated with different colors. Holocene
 993 marine unit and lacustrine unit are shown by blue and green color, respectively. Core CS-01
 994 penetrates the upper half of the Holocene marine muds based on the core-to-seismic correlation.
 995 The wedge out of the marine sediments is obscured at NNAF close to NE of the profile.

996 **Fig 4.** Generalized sedimentary log of core CS-01 and radiographic images, showing the main
 997 lithostratigraphy of the Holocene marine unit deposited during the last 6.1 cal kyrs BP (Fig. 5).
 998 According to visual sedimentological observation on the core, we differentiated 28
 999 seismoturbidite layers (ST-1 to ST-28), intercalating with hemipelagic/pelagic sediments. Red
 1000 color within seismoturbidite unit represents the basal coarse-grained part, blue colored layers
 1001 represent amalgamated turbidites, whereas yellow color is assigned to a homogenite part. Red
 1002 stars indicate the ^{14}C sample locations with calibrated ages.

1003 **Fig 5.** Age-depth model for background sediment of the core CS-01 are reconstructed based on
1004 seven AMS ^{14}C ages by using Bacon.r Script. Red line represents the mean age of the iterations.
1005 Blue diamonds are the levels of the ^{14}C samples. Grayscale background indicates the iteration
1006 distribution. Black dash lines represent the position of the ST units.

1007 **Fig 6.** Color image and radiography of the selected seismoturbidite layers (ST-4 and ST-13,
1008 249 cmbsf and 957 cmbsf from base respectively) together with correlative plots of MS, gamma
1009 density, elemental profiles (Mn/Ca, Fe/Ca, Ca, K, Sr) and combination of grainsize parameters
1010 (sorting, skewness, ratios of clay, silt and sand). Secondary sorting profile is focused on the
1011 background sediment and homogenite transition.

1012 **Fig 7.** Color image and radiography of the selected amalgamated seismoturbidite layers (ST-6
1013 and ST-7, 336 cmbsf and 460 cmbsf from base respectively) together with correlative plots of
1014 MS, gamma density, elemental profiles (Mn/Ca, Fe/Ca, Ca, K, Sr) and combination of grainsize
1015 parameters (sorting, skewness, ratios of clay, silt and sand).

1016

Fig 1

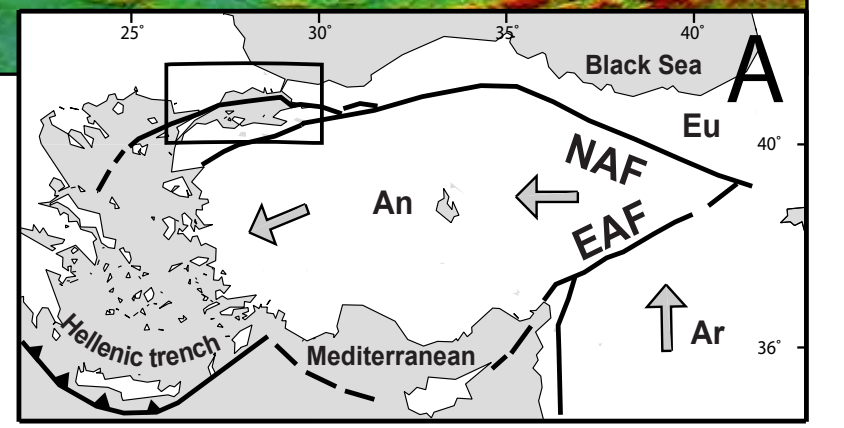
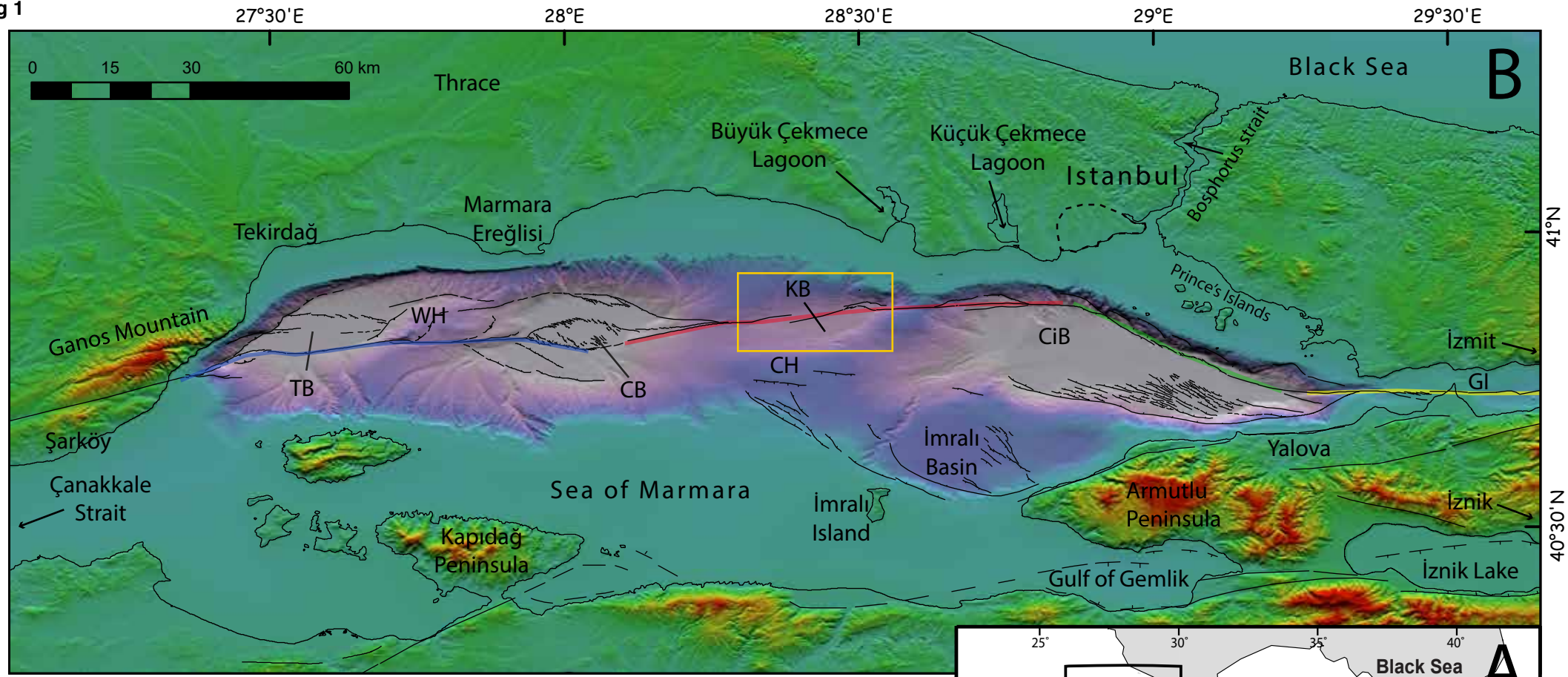


Fig 2

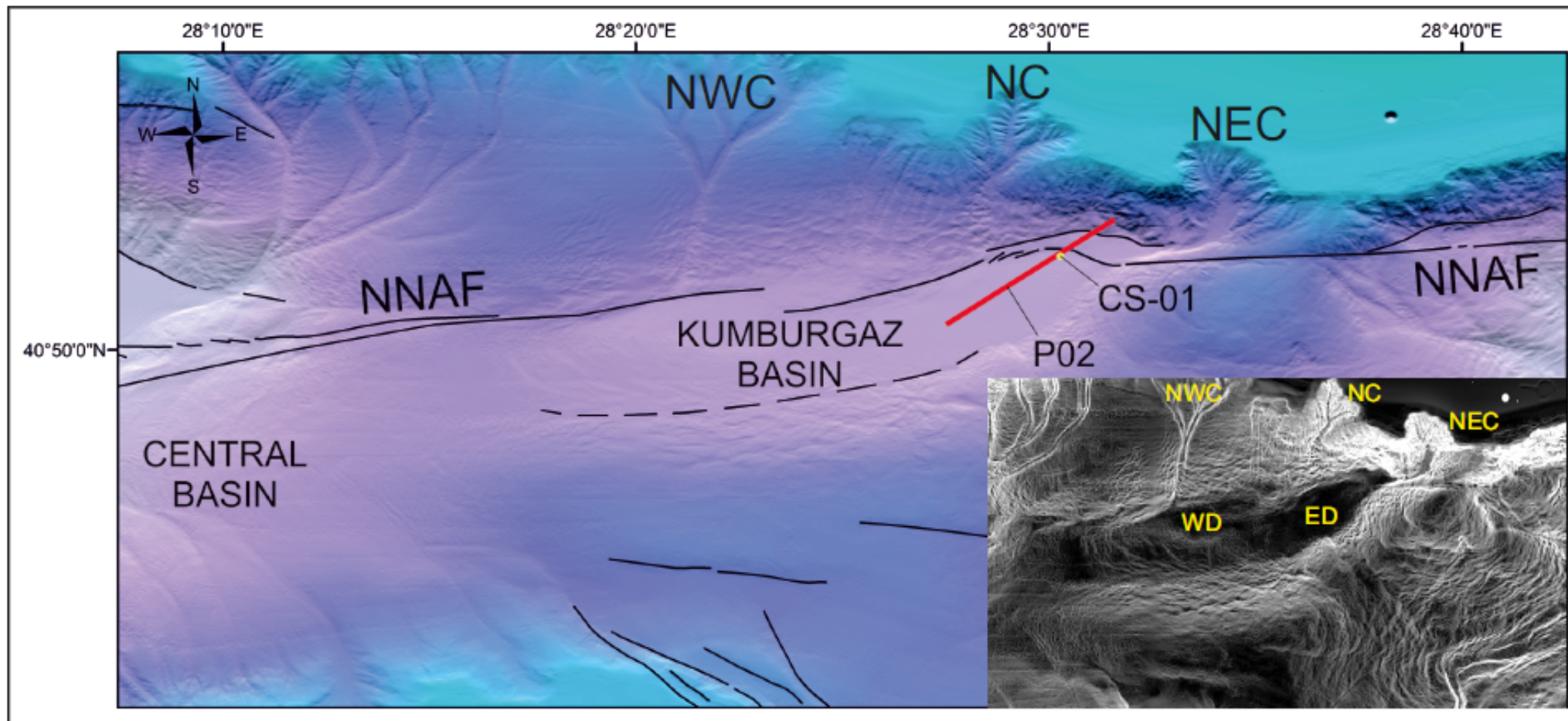


Fig 3

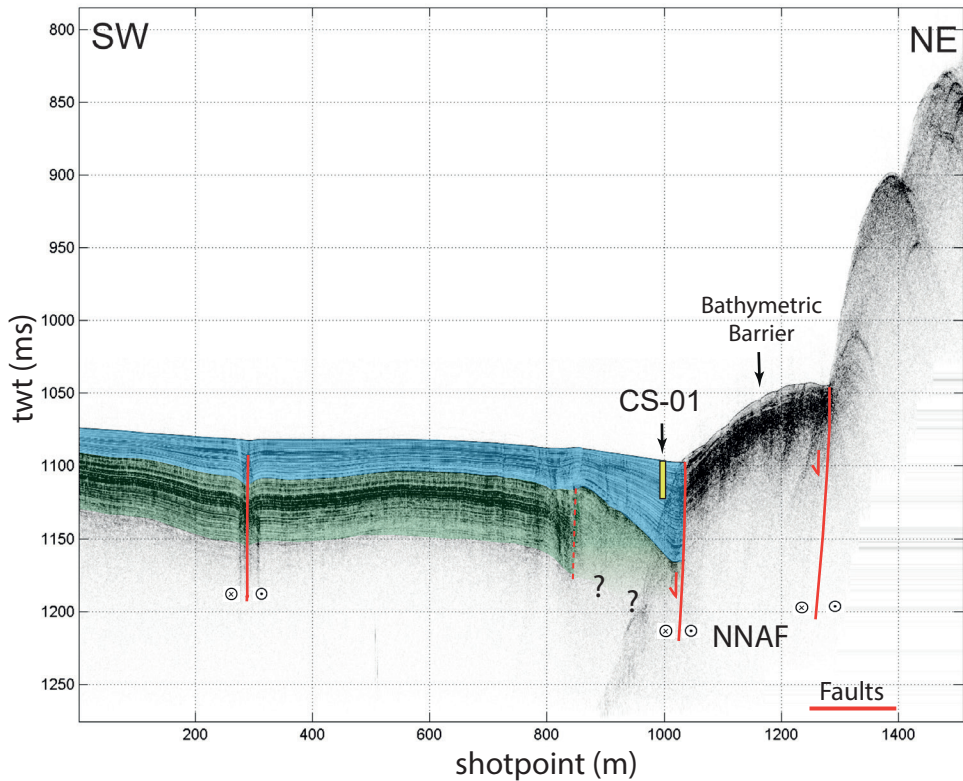


Fig 5

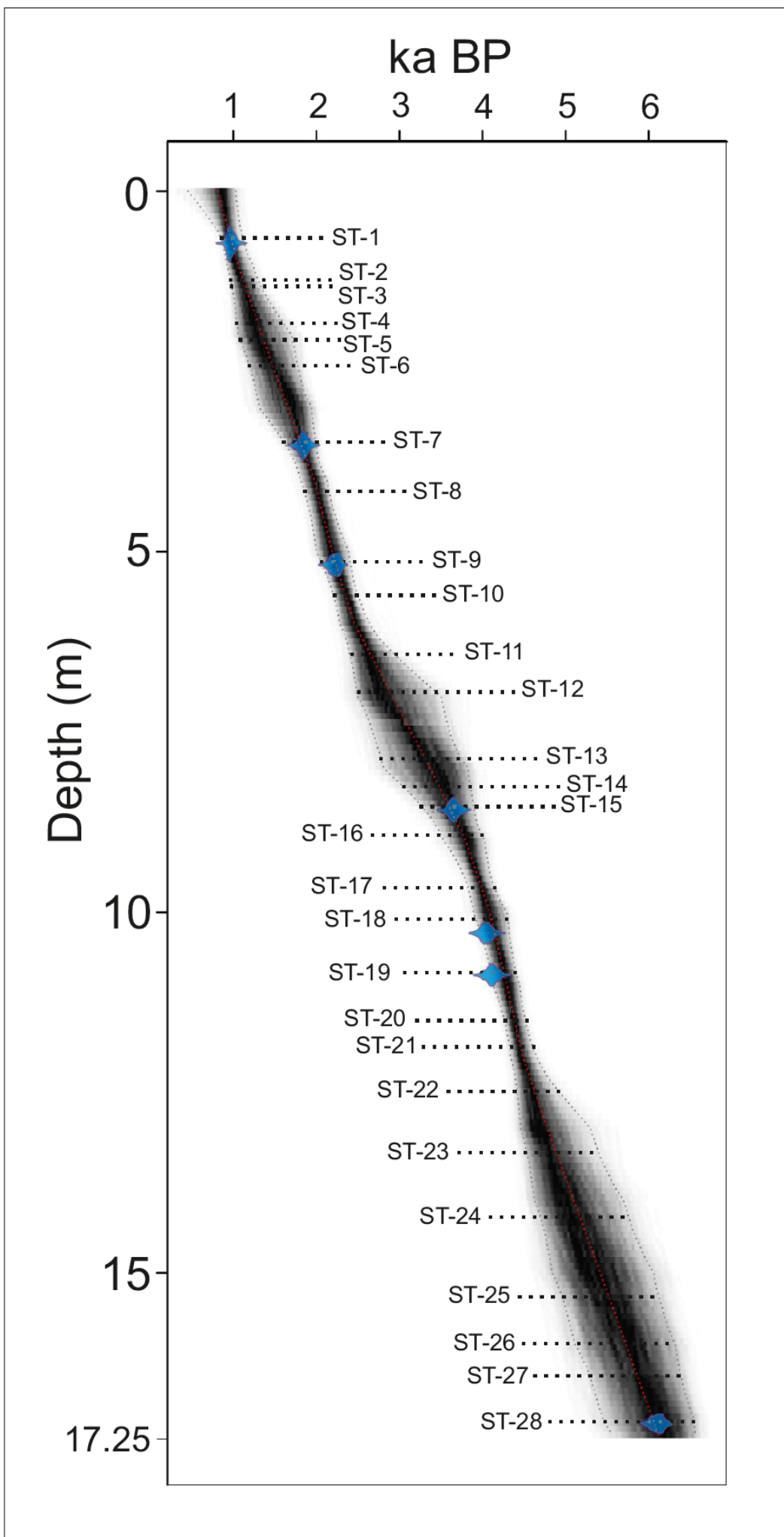


Fig 6

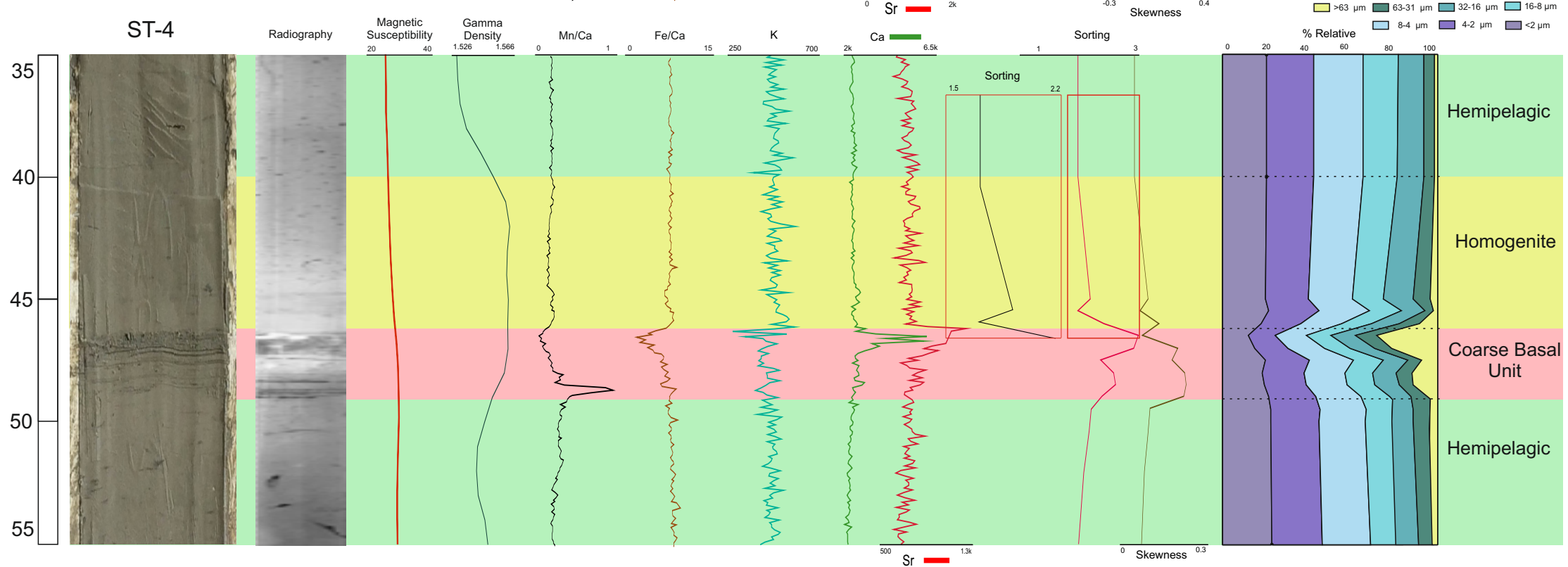
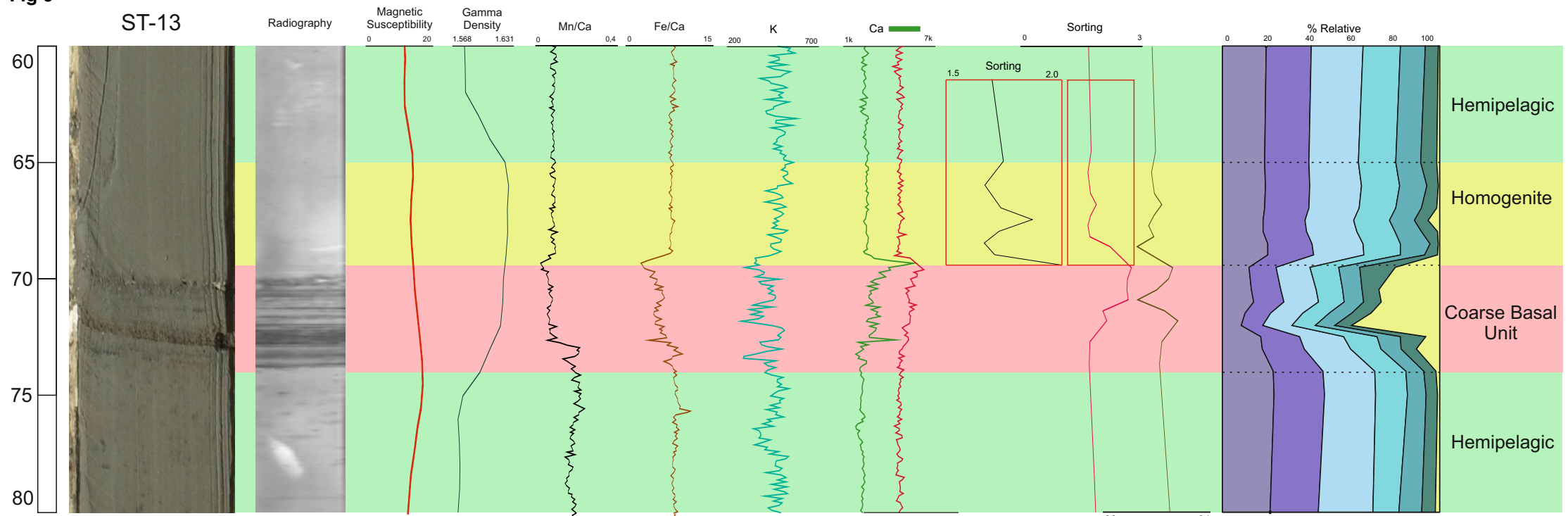


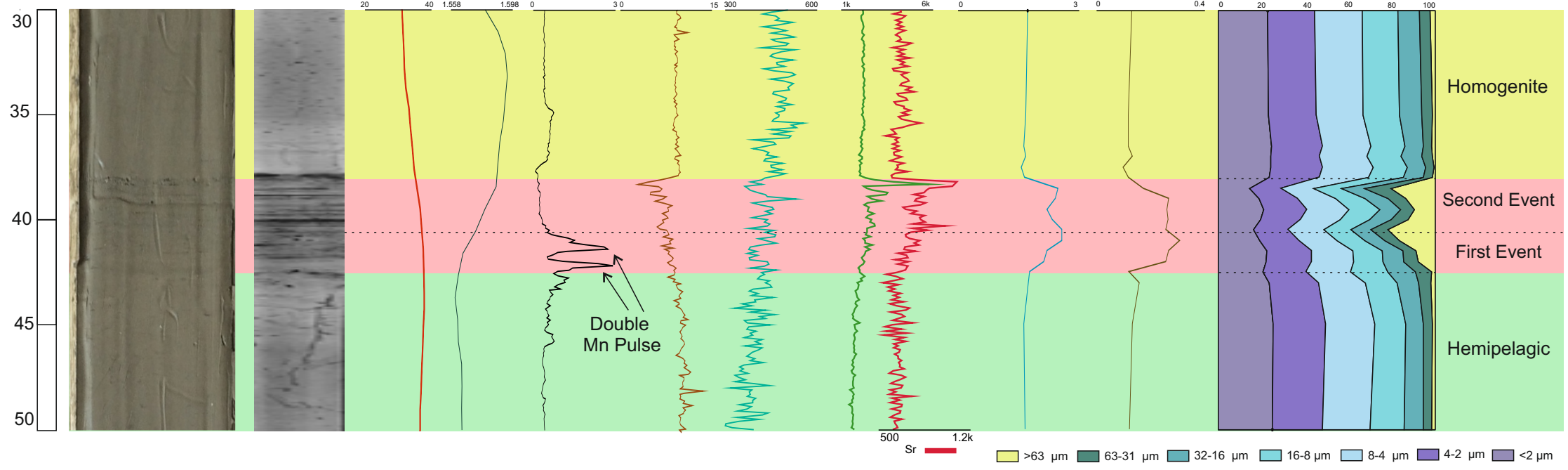
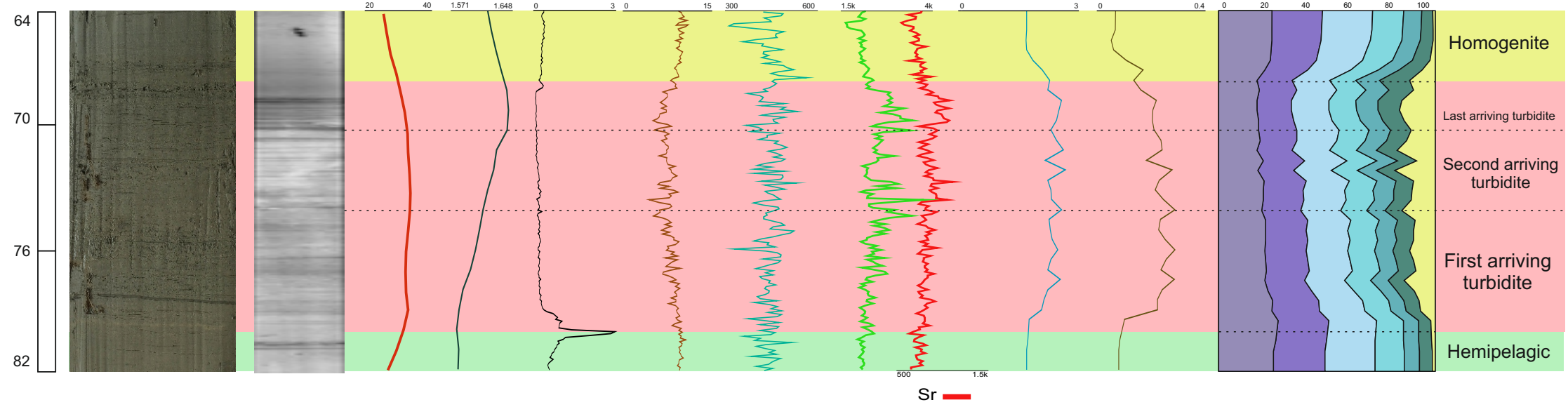
Fig 7**ST-6****ST-7**

Table 1. Summary of AMS radiocarbon dates obtained from core CS-01. Reservoir correction applied as $\sim 390 \pm 85$ yrs. according to [Siani et al. \(2000\)](#).

Sample Name	Depth in Core (mm)	Depth in background	Uncalibrated age (BP)	Calibrated age (BP)
Age 1	1300	725	1505 \pm 30	974 \pm 71
Age 2	4639	3526	2325 \pm 35	1836 \pm 103
Age 3	6535	5181	2640 \pm 35	2223 \pm 94
Age 4	10469	8584	3815 \pm 35	3666 \pm 113
Age 5	12539	10291	4115 \pm 35	4041 \pm 121
Age 6	13155	10848	4160 \pm 35	4105 \pm 123
Age 7	20910	17092	5780 \pm 45	6100 \pm 127

Table 2. Seismoturbidite age ranges based on age-depth model (Fig. 5).

ST number	Depth (mm)	Mean (AD/BC)
1	1200	964,8 AD
2	1780	820,5 AD
3	1899	796,7 AD
4	2495	658,6 AD
5	2870	578,4 AD
6	3367	464 AD
7	4605	135,9 AD
8	5390	63,5 BC
9	6510	284,3 BC
10	7119	420,4 BC
11	7950	701,4 BC
12	8624	982,9 BC
13	9577	1374,5 BC
14	10140	560,3 BC
15	10440	1658,4 BC
16	10965	1842 BC
17	11840	2060 BC
18	12505	2190,7 BC
19	13140	2308,4 BC
20	14185	2444,9 BC
21	14605	2517,6 BC
22	15320	2687,2 BC
23	16405	2957 BC
24	17490	3248,4 BC
25	18755	3576,5 BC
26	19645	3797 BC
27	20165	3915,2 BC
28	20875	4111,2 BC

Table 3. Distribution of historical earthquakes and seismoturbidites found in CS-01 in correlation with other seismoturbidite based studies in the SoM. Abbreviations: a) [McHugh et al., 2006](#), b) [McHugh et al., 2014](#), c) This study, d) [Drab et al., 2015](#), e) [Çağatay et al., 2012](#), respectively. Note that, assigned letters corresponds the ST units that have been correlated with historical earthquakes.

Central Basin	Kumburgaz Basin	Çınarcık Basin	Gulf of Izmit
		1894 AD (d)	
		1509 AD (d)	1509 AD (e)
1343 AD (a,b)		1343 AD (d)	
			1296 AD (e)
	989 AD (c) (ST1)	989 AD (d)	
860-865 AD (b)	869 AD or 862 AD (c) (ST2)		860-865 AD (e)
740 AD (a)	740 AD (c) (ST3)	740 AD (d)	740 AD (a,e)
557 AD (b)	557 AD or 554 AD (c) (ST4)		
	447 AD or 478 AD (c) (ST5)	478 AD (d)	
	407 AD (c) (ST6)		358 AD (e)
268 AD (b)			268 AD (e)
	120-128 AD or 180-181 AD (c) (ST7)		180-181 AD (a)
	29 AD or 69 AD (c) (ST8)		
	287 BC or 427 BC (c) (ST9)		427 BC (e)